NASA TECHNICAL NOTE

NASA TN D-2027

CHARACTERISTICS OF A LUNAR LANDING CONFIGURATION HAVING VARIOUS MULTIPLE-LEG LANDING-GEAR ARRANGEMENTS

by Ulysse J. Blanchard

Langley Research Center
Langley Station, Hampton, Va.

NATIONAL AERONAUTICS AND SPACE ADMINISTRATION • WASHINGTON, D. C. • JANUARY 1964

CHARACTERISTICS OF A LUNAR LANDING CONFIGURATION HAVING VARIOUS MULTIPLE-LEG LANDING-GEAR ARRANGEMENTS

By Ulysse J. Blanchard

Langley Research Center
Langley Station, Hampton, Va.

Technical Film Supplement L-803 available on request.

NATIONAL AERONAUTICS AND SPACE ADMINISTRATION

For sale by the Office of Technical Services, Department of Commerce,
Washington, D.C. 20230 -- Price $1.25

NATIONAL AERONAUTICS AND SPACE ADMINISTRATION

TECHNICAL NOTE D-2027

CHARACTERISTICS OF A LUNAR LANDING CONFIGURATION HAVING VARIOUS MULTIPLE-LEG LANDING-GEAR ARRANGEMENTS

By Ulysse J. Blanchard

SUMMARY

An experimental investigation has been made of some lunar-landing characteristics of a 1/6-scale dynamic model of a landing module having multiple-leg landing-gear systems. Symmetric four-point and five-point systems and an asymmetric four-point system were investigated. The landing-gear legs were inverted tripod arrangements having a telescoping main strut which incorporated a yielding-metal strap for energy dissipation, hinged V-struts, and circular pads. The landing tests were made by launching a free model onto an impenetrable hard surface (concrete) and onto a powdered-pumice overlay of various depths. Landing motion and acceleration data were obtained for a range of touchdown speeds, touchdown attitudes, and landing-surface conditions.

Maximum normal acceleration experienced at the module center of gravity during landings on hard surface or pumice was 2g (full-scale lunar value in terms of earth's gravity) over a wide range of touchdown conditions. Maximum angular acceleration experienced was $12\frac{1}{2}$ radians/sec^2 and maximum longitudinal acceleration was $1\frac{3}{4}$g. The module was very stable with all gear configurations during landings on hard surface (coefficient of friction, $\mu = 0.4$) at all conditions tested. Some overturn instability occurred during landings on powdered pumice ($\mu = 0.7$ to 1.0) depending upon flight path, pitch and yaw attitude, depth of pumice, surface topography, and landing-gear configuration. The effect on stability of roll attitude for the limited amount of roll-attitude landing data obtained was insignificant. Compared with the four-point landing gear, the five-point system with equal maximum gear radius increased landing stability slightly and improved the static stability for subsequent lunar launch. A considerable increase in landing stability in the direction of motion was obtained with an asymmetric four-point gear having two pads offset to increase gear radius by 33 percent in the direction of horizontal flight. Author

INTRODUCTION

Two of the important items for overall success of the Apollo mission are a soft, stable landing of a manned spacecraft on the lunar surface and subsequent departure from the lunar surface. The landing-gear systems must arrest and stabilize the landing module, provide a stable support on the lunar surface, and also provide an adequate platform from which to launch a return stage. Proposed control and guidance capabilities indicate that favorable module touchdown conditions (attitude, orientation, and speed) can be achieved along with limited site selection (hover). However, knowledge of detailed lunar-surface characteristics is lacking and only generalized assumptions can be made from current literature and experimentation. Therefore, currently proposed landing-gear systems are designed to accomplish the task for a fairly wide range of landing-surface conditions with minimum weight and operational complication. Multiple-point leg systems with simple nonviscous, low-rebound shock absorbers are promising with regard to these general requirements and capabilities.

Results are presented herein of an investigation of a 1/6-scale dynamic model of a manned spacecraft for soft lunar landing (a preliminary version of the lunar excursion module) employing a multiple-point, leg-type landing-gear system with yielding-metal shock absorbers and several contact-point arrangements. Impact acceleration and behavior were determined with a 1/6-scale dynamic model over a range of touchdown speeds and attitudes. The landing-surface configurations investigated included a smooth hard surface, various depths of dust overlay, and an integrated surface irregularity.

Motion pictures of typical landings were made during the tests and film supplement L-803 showing these results is available on loan from the NASA. A request card and a description of the film are provided at the end of this paper, on the page with the abstract cards.

SYMBOLS

A	area, sq ft
a	acceleration, ft/sec^2
α	angular acceleration, $radians/sec^2$
β	gravitational ratio, g_{earth}/g_{moon}
F	force, lb
γ	flight-path angle, deg
I	moment of inertia, $slug\text{-}ft^2$

l	length, ft
λ	geometric model scale
m	mass, slug
σ	stress, lb/sq in.
t	time, sec
μ	coefficient of friction
V	velocity, ft/sec
V_H	horizontal velocity, ft/sec
V_V	vertical velocity, ft/sec
V_R	resultant velocity, ft/sec

DESCRIPTION OF MODEL

The general arrangement of the 1/6-scale dynamic model is shown in figure 1. Photographs of the model with various landing-gear configurations are shown in figures 2, 3, and 4. Details of the inverted tripod landing-gear leg assembly and yielding-metal shock absorber are shown in figure 5. Full-scale and model-scale relationships applicable to these tests are given in table I. Pertinent model and full-scale dimensions are given in table II.

The model was a symmetrical body about the vertical axis representing a lunar landing module consisting of the landing stage with attached landing gear and the lunar launch stage. The model was constructed of a solid hardwood and balsa core containing appropriate cavities for instrumentation and ballast. The model body was covered with a plastic-impregnated fiber-glass skin. Landing-gear assemblies were made of 2024-T3 aluminum alloy. The gear struts were of tubing of 0.065-inch wall thickness with 5/8-, 1/2-, and 3/8-inch outside diameter for the main strut, inner slide, and V-strut, respectively.

The basic landing gear (figs. 1, 2, and 3(a)) was a quadruped configuration with each of the four legs (fig. 5) consisting of three struts mounted so as to form an inverted tripod. The landing gear was designed to provide stroke for a desired maximum acceleration and residual clearance for engine-nozzle protection and subsequent launch capability. Vertical working stroke of the gear was approximately 2 feet full scale and was designed to give a maximum load of 2 earth g for a flat impact at a speed of 15 feet per second. A balsa block (stop) at the top of the main strut provided an emergency stroke of approximately 3 additional

inches. The main or upper strut telescoped during impact and the lower V-strut was a hinged unit, which served to guide and stabilize the tripod. During impact the telescoping main strut yielded a metal energy strap in tension for impact attenuation. Also, as the main struts telescoped, the landing pads moved outward and thus increased the gear diameter as shown in figure 1. The pads were attached to the tripod assembly by a ball joint with no provision for shock absorption in the pads. Two footprint areas of the landing-gear pads were utilized, as indicated in table II.

The modified landing-gear configurations investigated are shown in figures 3(b) and 4. The asymmetric four-point gear (fig. 3(b)) was similar to the basic symmetric four-point gear but with two adjacent pads offset radially 3 feet (full scale). This offset increased gear radius approximately 33 percent in the direction of offset. Gear height was held constant and the energy-strap shock-absorber configuration was unchanged.

The five-point landing gear shown in figure 4 was symmetrical with a 72° circumferential spacing. All gear and strut dimensions were the same as those of the symmetrical four-point arrangement. Therefore, maximum gear radius was the same and minimum gear radius was increased approximately 15 percent. The energy straps were modified to provide the same design load as that of the four-point system.

The model energy straps were made of pure nickel wire (Low-Carbon Nickel) a highly ductile metal which retains its mechanical properties over a wide range of temperatures. During impact, compression loads tending to telescope the main strut were opposed by the energy strap in tension. When the load exceeded the yield strength of the strap, it elongated and the gear stroked. Because of yield of the ductile metal, little energy was stored; and rebound was thus minimized. Stress-strain characteristics of the strap material were similar to those described in reference 1, and a typical stress-strain diagram for Low-Carbon Nickel is shown in figure 6. The shock-absorber element used on the present model had desirable characteristics for the lunar-landing mission, but these characteristics could also be obtained by using other methods such as crushable materials, frangible tubes, or properly designed oleo systems.

The scale ralationships pertinent to the earth model tested are shown in table I. For geometric scaling the characteristic length was varied as the scale factor λ. A 1/6-scale model was chosen, since this choice was suitable for meeting construction, size, and weight requirements for test purposes. The same yield-strap material was assumed for the model and the full-scale configurations; hence, the stress relationship was held 1 to 1, so that exact structural scaling of shock-absorber forces was provided. The gravitational ratio β is dictated by the fact that the force of the earth's gravity is 6 times that of the moon; thus, accelerations experienced by the model are 6 times that resulting on the moon. With these three relationships fixed, other pertinent scale relationships follow from laws of physics for a dynamically scaled model.

APPARATUS AND PROCEDURE

The investigation was conducted by launching the model as a free body by means of a pendulum apparatus in the Langley impact structures facility. The model is shown on the pendulum launching carriage in figure 7. Operation of the pendulum during landing tests is illustrated in figure 8. The pendulum with the model locked at the desired attitude was retracted to the point A, from which it was released and allowed to swing through an arc of vertical height AB. Model release occurred at point B (dead center) at a horizontal velocity V_H approximately equal to a free-fall velocity for preset vertical distance AB. After release the model dropped a preset height BC for desired vertical velocity V_V. The combination of horizontal velocity at release and vertical velocity at impact determined flight-path trajectory at model touchdown. A photograph showing the pendulum, support structure, and pumice box installed in the Langley 41-foot vacuum sphere is shown in figure 9.

Pitch and roll attitudes (about the axes shown in fig. 2) were obtained by a multiple platform and hinge arrangement mounted beneath the pendulum carriage (fig. 7). The model pitch attitude was obtained by setting the support release mechanism to the desired angle on the pitch quadrant. Roll attitude was similarly obtained with a quadrant located on the side of the carriage. Yaw attitude was obtained by rotating the clevis fitting installed on top of the model (figs. 2, 3, and 4). Negative pitch attitude was obtained by rotating the entire carriage assembly 180°. Combinations of pitch, yaw, and roll could also be obtained.

The landing surfaces used for the investigation are diagramed in figure 10. Hard-surface landings were made on smooth concrete and hardwood. The ledge simulated a dropoff or crevice of about 2 feet (full scale). Simulated landings in lunar dust were made into a shallow box containing $\frac{7}{8}$, $1\frac{3}{4}$, and $3\frac{1}{2}$ inches of powdered pumice representing full-scale depths of 5, $10\frac{1}{2}$, and 21 inches, respectively. The grain-size distribution of the pumice material is shown in figure 11. Average grain size of the powdered pumice was approximately 68 microns (400 microns full scale). Grain geometry was random, sharp edged, and jagged. The pumice was disturbed and loosely struck off level (minimum compaction) before each landing. Static bearing strength of the pumice during model tests was approximately 2 lb/sq in. with a bulk density of approximately 40 lb/cu ft. Bearing strength was measured with a spring-scale penetrometer provided with a 1.0-inch-diameter cylindrical footing and a 1/4-inch penetration in a 4-inch depth of pumice. A few check landings were made in pumice having bearing strengths up to approximately 10 lb/sq in. In general, these surface conditions were similar to those of the NASA Manned Spacecraft Center lunar-surface model.

Landing-impact accelerations were measured by strain-gage accelerometers rigidly mounted in the model as shown in figure 12. The accelerometers were mounted on a common base which could be rotated in line with the axis of flight, depending upon model yaw attitude. Normal acceleration at the center of gravity was measured with a 20g accelerometer. Longitudinal acceleration was measured with a 15g accelerometer mounted above the normal accelerometer. Angular

acceleration was measured with a pair of matched 50g accelerometers. The natural frequency was about 180 cycles per second for the 15g and 20g accelerometers and about 310 cycles per second for the 50g accelerometers. The accelerometers were damped to 65 percent of critical damping. The response of the recording galvanometers was flat to about 190 cycles per second for the 15g accelerometers and to about 135 cycles per second for the 20g and 50g accelerometers. A trailing cable, supported by an overhead guide wire, was used to transmit accelerometer signals to an oscillograph. Total gear stroke was obtained by measuring linear elongation of the energy straps after each landing. Impact points, slideout, and penetration characteristics (in pumice) were visually observed and measured. Motion-picture cameras recorded general behavior during landings.

The orientations of acceleration axes, attitudes, and the flight-path angles during landings are shown in figure 13. Landings were made at touchdown pitch attitudes of -15° to $+15^\circ$, yaw attitudes of 0° (one gear leg forward) and 36° or 45° (two legs forward), roll attitude of 15°, and combinations of the above. Vertical landing speed was varied from 5 to 15 feet per second and horizontal speed was varied from 0 to 15 feet per second (full scale). Combinations of vertical and horizontal speed result in touchdown flight-path angles ranging from approximately 26° to 90°. (See table in fig. 13.) The landings were made at a model weight corresponding to a full-scale lunar weight of 1,333 pounds (8,000 lb earth weight). The sliding coefficient of friction during hard-surface landings (concrete or wood) was about 0.4 and was about 0.7 to 1.0 on the powdered pumice overlay. In general, landing tests of the basic four-point gear were made over the entire range of parameters, whereas the asymmetric four-point and the symmetric five-point gears were investigated only at conditions where instability had occurred with the basic gear. The footprint bearing area of the landing-gear pad was varied by a factor of 4 during landings in pumice.

In order to determine the effect of entrainment of air and moisture in the powdered pumice on landing stability of the model a few landings were made in a vacuum of 0.20 millimeter of mercury. During the landing tests under vacuum a mechanical shaker mounted on the chamber floor was used in an effort to settle the pumice during evacuation.

RESULTS AND DISCUSSION

All impact data presented are converted to full-scale lunar values in terms of the earth's gravitational constant by use of the scale relations given in table I.

Symmetric Four-Point Landing Gear

Hard-surface landings.- Oscillograph records showing typical impact characteristics during landings on a flat hard surface are shown in figure 14 for various landing speeds and attitudes with the symmetric four-point gear. Impacts were generally characterized by one or two main impulses, depending upon contact attitude, followed by secondary loadings due to very small rebounds which were damped in 2 or 3 cycles.

Landing impacts: Maximum accelerations experienced during such landings are plotted against flight-path angle for various pitch and yaw attitudes in figure 15. The module experienced little change in maximum acceleration with change in flight-path angle from 33° (V_V = 10 ft/sec; V_H = 15 ft/sec) to 90° (V_V = 15 ft/sec; V_H = 0 ft/sec). Maximum normal acceleration (2g) actually occurred at a pitch attitude of 0° and a flight-path angle of 90° when all landing-gear shock absorbers yielded simultaneously and equally. Maximum accelerations are plotted against touchdown pitch attitude in figure 16 for landings at a flight-path angle of 45° on flat and ledged hard surfaces at yaw angles of 0° and 45°. Normal and longitudinal accelerations did not change significantly with variation in pitch attitude from -15° to +15°. During landings at positive pitch attitude (+15°), the module with horizontal velocity underwent a positive longitudinal acceleration at touchdown as noted in figures 14, 15, and 16. This acceleration resulted from the relative motion and friction between the trailing pad or pads and the landing surface during the impact stroke, when the trailing pad displaced rearward over the surface. A similar reaction occurred for a flight-path angle of 90° and a positive or negative pitch attitude (fig. 15). Maximum longitudinal acceleration was approximately $\frac{1}{2}$g during hard-surface landings.

Angular accelerations during landings on a flat hard surface increased from a maximum of approximately $6\frac{1}{2}$ radians/sec^2 at 0° pitch attitude to $12\frac{1}{2}$ radians/sec^2 with increase in pitch to ±15°, as shown in figures 15 and 16. Angular acceleration also increased slightly with change in yaw attitude from 0° to 45° during landing at pitch attitude. For landings astride the ledge at a pitch attitude of 0° (fig. 16), angular accelerations were about the same as for landings at pitch attitudes of ±15° on the flat surface.

The data plotted in figure 16(a) for a landing astride the ledge at pitch and yaw attitudes of 0° were obtained during the sequence illustrated in figure 17(a) with three legs impacting on the ledge. In this case all four legs absorbed energy. Severe loading of a single leg was obtained for the condition illustrated in the sequence of figure 17(b). Essentially, only two legs were involved in this case and high accelerations resulted when the leading-leg shock absorber was bottomed; that is, the emergency balsa stop was crushed.

The possibility of all impact energy being imposed on a single leg suggests the desirability of increased available stroke or stiffer shock absorbers for the present system. Maintaining low gear forces and increasing the stroke would be preferable from an overturn stability standpoint. A varying-force shock-absorber system (pyramided force levels) has been suggested in an unpublished analysis made by Charles C. Filley at the NASA Manned Spacecraft Center. In the suggested system four force levels, increasing with stroke, are available in each of the four legs and a single leg has the same design energy-dissipating capability for full stroke as four legs using one-quarter stroke. Such a system would be effective and would reduce stroke requirements as compared with the present system for a single-leg impact.

Another system would link all articulating legs to a single shock-absorber unit or element, and deflection of any number of legs (single or multiple) would

provide the same energy-dissipating capability for the same stroke. The shock absorber could be a constant- or variable-force system.

Maximum accelerations obtained during hard-surface landings at a roll attitude of 15° are presented in table III. When compared with the data in figures 15 and 16, acceleration values and trends at a roll attitude of 15° were generally similar to those at a roll attitude of 0°.

Landing stability: During landings on a flat or a ledged hard surface, the module appeared very stable with regard to overturning for all landing conditions tested. Slideout distances in the order of 30 to 40 feet (full scale) resulted at the highest horizontal speed (15 ft/sec). At a yaw attitude of 0° where one leg is forward, an undamped pitching oscillation occurred during slideout as illustrated by the oscillograph record in figure 18(a). Greater stroking of the leading leg as compared with that of the side and rear legs during impact at a yaw attitude of 0° was caused by a combination of pad friction and landing dynamics. This phenomenon resulted in an unsteady or teetering platform during slideout and subsequently at rest. Landing at a yaw attitude of 45° where two legs are forward generally alleviated this characteristic. (See fig. 18(b).) Landings at a roll attitude of 15° did not affect overturn stability. (See table III.) Some teetering was noted during landing slideouts for landings at a roll attitude.

Dust-surface landings.- Oscillograph records showing typical impact characteristics during landings on a flat dust overlay 21 inches deep are shown in figure 19 for various landing attitudes with the symmetric four-point gear. Impact events were generally similar to those on a hard surface (fig. 14). Inspection of figures 14(b) and 19(b) shows that in the 21-inch depth of dust, acceleration onset rate was reduced.

Landing impacts: Maximum accelerations experienced during landings in two depths of pumice dust are plotted against flight-path angle for various pitch and yaw attitudes in figure 20. Normal and longitudinal acceleration did not change appreciably with change of flight-path angle but angular acceleration increased in some cases with reduction of flight-path angle (increased horizontal speed). The depth of dust had no appreciable overall effect on maximum accelerations. Compared with the accelerations encountered in hard-surface landings (fig. 15) maximum normal accelerations in dust were relatively unchanged as a result of the use of an essentially constant-force shock-absorber system. However, negative longitudinal acceleration (drag) increased by a factor of 2 or 3 to approximately $1\frac{3}{4}g$ because of increased resistance to horizontal sliding in the dust.

During a landing at a pitch attitude of -15° and a flight-path angle of 30° (V_V = 8.7 ft/sec, V_H = 15 ft/sec) with one leg forward (0° yaw) the lower V-strut of the leading leg buckled at initial impact on that leg as indicated in figure 20(a). At this landing condition the main strut did not stroke; this result indicates that the resultant force of impact in the dust was vectored along or below the plane of the V-strut, so that excessive column loading and failure occurred. The landing was similar to stubbing the gear pad at touchdown on an immovable obstacle (rock or boulder). This result indicates the desirability of providing shock-attenuation capability in the horizontal plane either by

incorporating stroke in the gear pads (crushable pads) or in the lower struts (tri-strut attenuation).

Maximum accelerations are plotted against touchdown pitch attitude in figure 21 for landings at yaw attitudes of 0° and 45° and a flight-path angle of 45° on flat and ledged surfaces having various depths of dust overlay. A somewhat greater change in accelerations with change in pitch attitude is noted for the dust landings, particularly at a yaw attitude of 45°, as compared with that obtained during hard-surface landings (fig. 16). This result was largely due to greater changes in friction or drag forces on the pads for impacts in pumice dust, and these changes, in turn, affect gear actuation and stroking.

Maximum accelerations for landings at a roll attitude of 15° are presented in table III. A decrease of approximately 50 percent in normal and longitudinal acceleration is noted for the landing at a pitch attitude of -15° as compared with the acceleration for the same pitch condition at a roll attitude of 0° (fig. 20(b)).

Accelerations during limited landings in the 41-foot-diameter vacuum sphere at 0.20 millimeter of mercury were similar to those at atmospheric pressure.

Landing stability: Unstable landings are indicated by the solid symbols in figures 20 and 21. The module was stable over a wide range of landing conditions during landings on the dust overlay. Overturning generally occurred at flight-path angles of 45° or less, depending upon module orientation (yaw attitude) and touchdown pitch attitude during landings on flat dust overlay. The module was most likely to overturn at 45° yaw attitude (minimum gear radius) and at -15° pitch attitude. However, at a yaw attitude of 0° (maximum gear radius) where one leg was forward, a misalinement relative to the velocity vector could cause the module to veer to a two-legs-forward orientation (45° yaw) with consequent overturning as indicated in figure 20(a) for a pitch attitude of 0° and a flight-path angle of 33°. Some teetering characteristics were noted during landings on powdered pumice at a yaw attitude of 0° as was the case for hard-surface landings. On the ledged surface, overturning occurred for all pitch conditions at 45° yaw with the symmetric four-point gear (fig. 21). The conditions for a yaw attitude of 0° were not tested on the ledge to avoid possible damage to the model gear such as that noted in figure 20(a).

The effects on landing stability of depth of dust and pad size are shown in figure 22. Data for two pad sizes and depths of dust are plotted at the flight-path angles at which instability occurred. At a touchdown pitch attitude of -15°, the module was unstable regardless of pad size or depth of dust tested. At a pitch attitude of 0° the module was stable in the 5-inch depth and unstable in the 21-inch depth of dust regardless of pad size. At a pitch attitude of 15°, mixed results occurred with the large pads either increasing or decreasing stability depending upon flight-path angle and depth of dust. Although inconclusive, the data indicate that in the shallow dust (5 inches), the large circular pads tested provided increased stability, whereas in the deep dust (21 inches) they were destabilizing. Both sets of pads tended to penetrate deeply and plow through the pumice during impact. The large pads penetrated at a flatter angle and not as deeply as the small pads. The small pads tended to penetrate through to the subsurface. When overturning occurred there was in most cases very little horizontal stroke or skidding of the leading pads during landing impact.

Overturn stability was generally unchanged during landings at a roll attitude of 15°. (See table III.) However, at a pitch attitude of -15° and a flight-path angle of 45°, the module was stable whereas at a roll attitude of 0°, it was unstable (fig. 20(b)). During rolled landings in the dust overlay the module tended to veer or rotate about the yaw axis at initial impact, but this effect did not seem to be a problem for these limited number of landings.

No changes in landing-stability characteristics were noted during landings in a vacuum environment of approximately 0.20 millimeter of mercury. It was observed that the pumice did not settle noticeably during evacuation of the sphere, and this result indicated that little compaction occurred. In this test dynamic penetration characteristics were not significantly changed because of the grain size and the vacuum pressure used. This is in agreement with the results presented in references 2 and 3.

Asymmetric Four-Point Landing Gear

Hard-surface landings.- Oscillograph records showing typical impact characteristics during landings on flat hard surface with the asymmetric four-point gear are shown in figure 23. Acceleration characteristics were similar to those for the symmetric four-point gear (fig. 14) except for small increases in acceleration pulse times and reduction in magnitudes due to the modified geometry. The change in geometry resulted in increased stroke during impact at the offset legs and the module generally came to rest pitched down in the direction of gear offset (forward). The maximum pitch attitude at rest was approximately 5° for the conditions tested.

Maximum accelerations experienced during three landings on flat hard surface with the asymmetric four-point gear are plotted in figure 16. Normal and longitudinal accelerations were the same as for the basic gear, and angular accelerations were reduced slightly.

Dust-surface landings.- Data obtained during landings with the asymmetric four-point gear on flat dust overlay are plotted in figure 24. Landing stability was increased considerably with the asymmetric gear as compared with the symmetric gear (fig. 20(b)). Likewise, stability was improved during landings on the ledged surface. See figure 21(b).

Maximum normal and longitudinal accelerations experienced with the asymmetric gear (fig. 24) were reduced relative to those experienced with the symmetric gear. Longitudinal accelerations during dust-surface landings were reduced as much as 50 percent. These reductions are attributed to the change in geometry of the offset legs which resulted in less "jamming" and more horizontal stroking of the leading pads through or over the dust during landing impact. This phenomenon is illustrated in figure 25 by typical oscillograph records showing landings on the ledge and dust overlay with the symmetric and asymmetric four-point gears. Particularly noticeable is the large change in time and magnitude of the longitudinal acceleration pulse at impact of the leading legs (which are labeled 2 to 3) and the associated change in horizontal displacement between the two gear configurations. Normal-acceleration pulses were similarly affected. The increased gear

radius and reduced pad loading of the asymmetric four-point gear were very effective in increasing landing stability.

Symmetric Five-Point Landing Gear

Hard-surface landings.- Maximum accelerations experienced during landings with the symmetric five-point landing gear on a flat hard surface are shown in figure 26 at various flight-path angles and landing attitudes. As expected, normal and longitudinal accelerations were approximately the same for this configuration as for the symmetric four-point gear. Angular accelerations at pitch attitudes were reduced slightly as a result of the reduced shock-absorber force of individual legs of the five-point system. For all landing conditions investigated, this configuration was stable. Slideout oscillations and static teetering encountered with the four-point system were generally eliminated, so that a more stable platform for lunar launching was provided.

Dust-surface landings.- Maximum accelerations experienced during landings with the symmetric five-point landing gear on flat dust overlay are shown in figure 27 at various flight-path angles and landing attitudes. In general, maximum accelerations were similar to those for the symmetric four-point system. The module was somewhat more stable during landings on dust overlay because of the net increase of approximately 15 percent in minimum gear radius, additional footprint, and reduced gear force.

CONCLUSIONS

Results of the dynamic-model investigation indicate that landing characteristics of a lunar landing module having multiple-point leg-type landing systems and yielding-metal shock absorbers were satisfactory over a considerable range of touchdown parameters and landing-surface conditions. The principal conclusions indicated by this investigation are as follows:

1. Maximum normal acceleration obtained during landings was approximately 2g (earth value) at the center of gravity. Maximum longitudinal acceleration on hard surface was approximately $\frac{1}{2}g$ and increased to approximately $1\frac{3}{4}g$ on powdered pumice overlay. Maximum angular acceleration was approximately $12\frac{1}{2}$ radians/sec^2 during hard-surface landings.

2. The module was very stable with regard to overturning with all landing-gear configurations during landings on an impenetrable hard surface (coefficient of friction, $\mu = 0.4$) at all conditions tested.

3. Some overturn instability occurred during landings on powdered pumice ($\mu = 0.7$ to 1.0) depending upon flight-path angle, touchdown attitude, depth of pumice, surface topography, and landing-gear configuration.

4. An asymmetric four-point gear configuration with two pads offset to increase gear radius by 33 percent in the direction of horizontal flight improved landing stability considerably on powdered pumice overlay.

5. A symmetric five-point gear configuration was slightly more stable than a four-point system with equal maximum radius and provides a nonteetering launch platform for lunar departure.

6. Shock attenuation capability in the horizontal plane would be desirable for extreme impact conditions.

Langley Research Center,
National Aeronautics and Space Administration,
Langley Station, Hampton, Va., August 16, 1963.

REFERENCES

1. Blanchard, Ulysse J.: Landing Characteristics of a Winged Reentry Vehicle With All-Skid Landing Gear Having Yielding-Metal Shock Absorbers. NASA TN D-1496, 1962.

2. Rowe, R. D., and Selig, E. T.: Penetration Studies of Simulated Lunar Dust. Trans. Seventh Symposium on Ballistic Missile and Space Technology, Vol. I, U.S. Air Force and Aerospace Corp., Aug. 1962, pp. 53-72.

3. Clark, Leonard V., and McCarty, John Locke: The Effect of Vacuum on the Penetration Characteristics of Projectiles Into Fine Particles. NASA TN D-1519, 1963.

TABLE I.- SCALE RELATIONSHIPS FOR EARTH MODEL OF LUNAR LANDING MODULE

λ = Geometric model scale

β = Gravitational ratio, 6
(g_{earth}/g_{moon})

Quantity	Lunar full scale	Scale factor	Earth model scale
Length	l	λ	λl
Stress (energy strap)	σ	1	σ
Acceleration	a	β	βa
Area	A	λ^2	$\lambda^2 A$
Force	σA	λ^2	$\lambda^2 F$
Mass	F/a	λ^2/β	$\frac{\lambda^2}{\beta}$ m
Velocity	$\sqrt{al}$	$\sqrt{\beta\lambda}$	$\sqrt{\beta\lambda}$ V
Time	V/a	$\sqrt{\lambda/\beta}$	$\sqrt{\lambda/\beta}$ t
Inertia	ml^2	λ^4/β	$\frac{\lambda^4}{\beta}$ I
Angular velocity	$1/t$	$\sqrt{\beta/\lambda}$	$\sqrt{\beta/\lambda}\ \omega$
Angular acceleration	$1/t^2$	β/λ	$\frac{\beta}{\lambda}\ \alpha$

TABLE II.- PERTINENT DIMENSIONS OF MODULE

	1/6-scale model	Full scale
General:		
Gross weight, lb	37.0	1,333
Moment of inertia (approximate):		
Roll, slug-ft^2	0.6	4,666
Pitch, slug-ft^2	0.6	4,666
Yaw, slug-ft^2	0.50	3,888
Overall height, ft	2.56	15.35
Overall diameter (basic gear):		
Small pads, ft	3.27	19.62
Large pads, ft	3.46	20.76
Center of gravity above ground line, ft	1.50	9.00
Landing gear:		
Symmetric four-point (four legs 90° apart):		
Maximum radius, ft	1.54	9.25
Minimum radius, ft	1.09	6.55
Vertical stroke, ft	0.35	2.10
Shock-strut energy strap (each):		
Cross-sectional area, sq ft	1.75×10^{-5}	6.28×10^{-4}
Length, ft	0.60	3.62
Asymmetric four-point (four legs 90° apart):		
Maximum radius:		
Basic legs (2), ft	1.54	9.25
Offset legs (2), ft	2.04	12.25
Minimum radius:		
Basic legs (2), ft	1.09	6.55
Offset legs (2), ft	1.44	8.65
Vertical stroke:		
Basic legs (2), ft	0.35	2.10
Offset legs (2), ft	0.47	2.80
Shock-strut energy strap (each):		
Cross-sectional area, sq ft	1.75×10^{-5}	6.28×10^{-4}
Length, ft	0.60	3.62
Symmetric five-point (five legs 72° apart):		
Maximum radius, ft	1.54	9.25
Minimum radius, ft	1.25	7.50
Vertical stroke, ft	0.35	2.10
Shock-strut energy strap (each):		
Cross-sectional area, sq ft	1.47×10^{-5}	5.30×10^{-4}
Length, ft	0.60	3.62
Gear pads:		
Small pad (each):		
Diameter, ft	0.19	1.13
Footprint area, sq ft	0.03	1.00
Large pad (each):		
Diameter, ft	0.38	2.25
Footprint area, sq ft	0.12	4.32

TABLE III.- RESULTS FOR ROLL ATTITUDE LANDINGS

Configuration	V_V, ft/sec	V_H, ft/sec	Flight-path angle, deg	Touchdown attitude			Surface		Maximum landing acceleration			Stability	
				Pitch, deg	Roll, deg	Yaw, deg	Hard	Dust depth, in.	Normal, g units	Longitudinal, g units	Angular, radians/sec^2	Stable	Overturn
Symmetrical four-point	10	10	45	0	15	45	√		1.3	-0.4	3.3 -1.3	√	
	10	10	45	15	15	45	√		1.1	0.3 -.4	8.9 -5.6	√	
	10	10	45	15	15	45	√		1.3	0.2 -.7	7.8 -6.0	√	
	10	10	45	-15	15	45	√		1.2	-0.3	5.4 -11.9	√	
	10	10	45	-15	15	0	√		0.9	-0.9	6.0 -7.4	√	
	10	10	45	0	15	45		5	1.2	-0.7	5.3 -3.0	√	
	10	15	33	0	15	45		5	0.9	-0.6	3.4 -4.2	√	
	10	15	33	0	15	45		21	0.7	-0.5	3.0 -2.1		√
	10	10	45	-15	15	45		5	1.0	-0.8	2.6	√	
	10	15	33	-15	15	45		5	1.0	-0.9	1.8		√
	10	15	33	0	15	0		5	1.0	-0.9	6.6 -2.4	√	
Asymmetrical four-point	10	10	45	15	15	45	√		0.8	0.2 -.5	8.0 -5.2	√	
	10	10	45	-15	15	45	√		0.8	-0.3	3.3 -8.4	√	
	10	10	45	-15	15	45	√		1.3	-0.4	3.2 -7.6	√	
	10	10	45	0	15	45	√		1.0	-0.4	4.3 -1.9	√	
Symmetrical five-point	10	10	45	0	15	0	√		1.3	-0.4	2.8 -2.4	√	

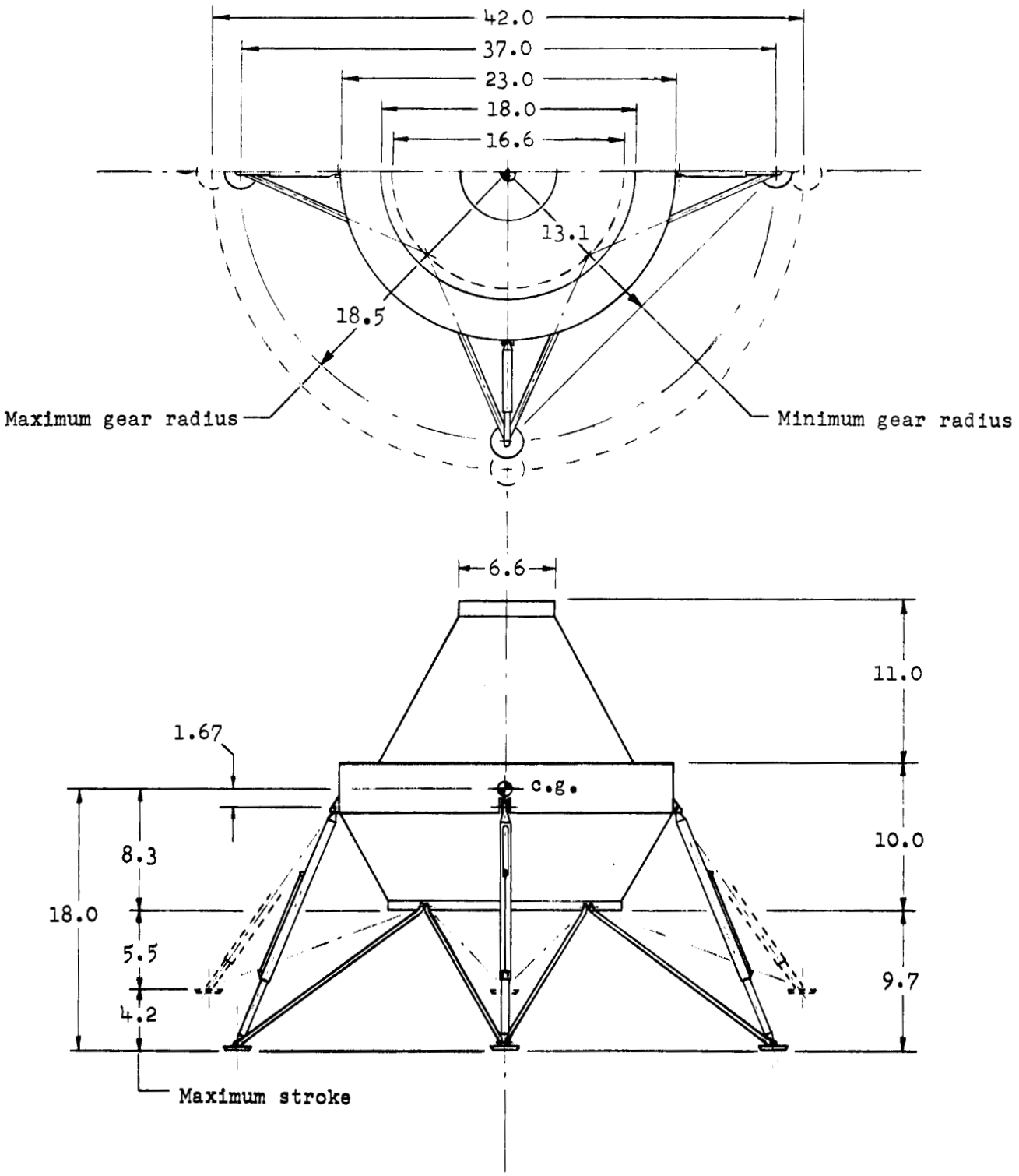

Figure 1.- General arrangement of 1/6-scale dynamic model. All dimensions are in inches.

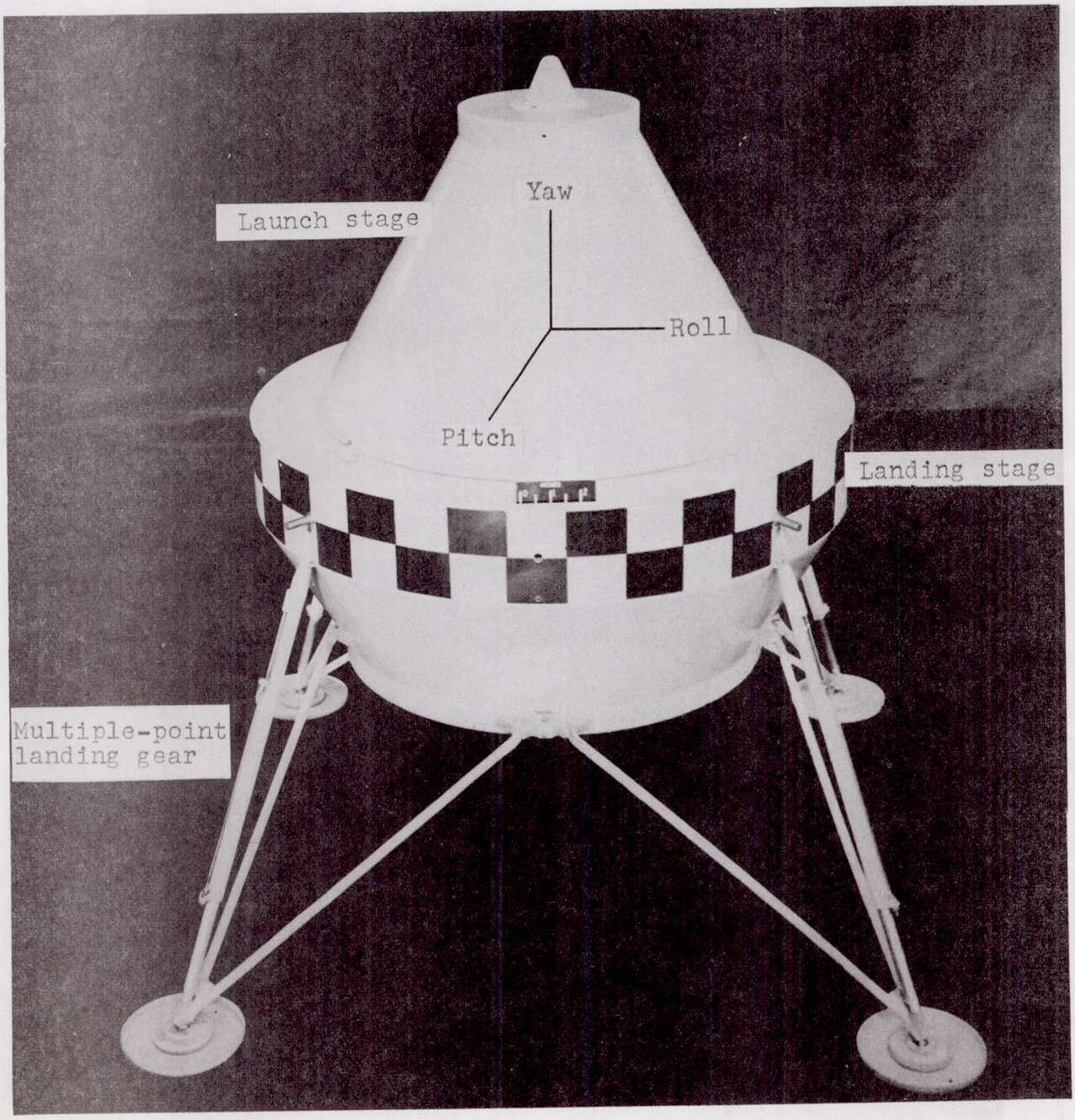

Figure 2.- Photograph of model with symmetric four-point landing gear. L-63-553.1

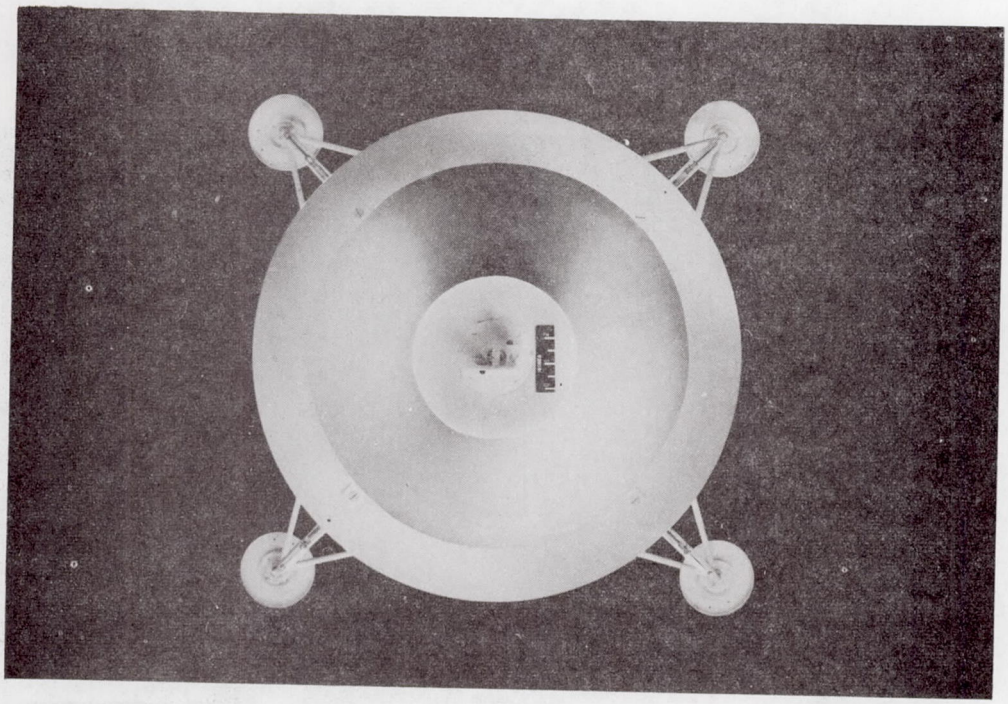

(a) Symmetric. L-63-554

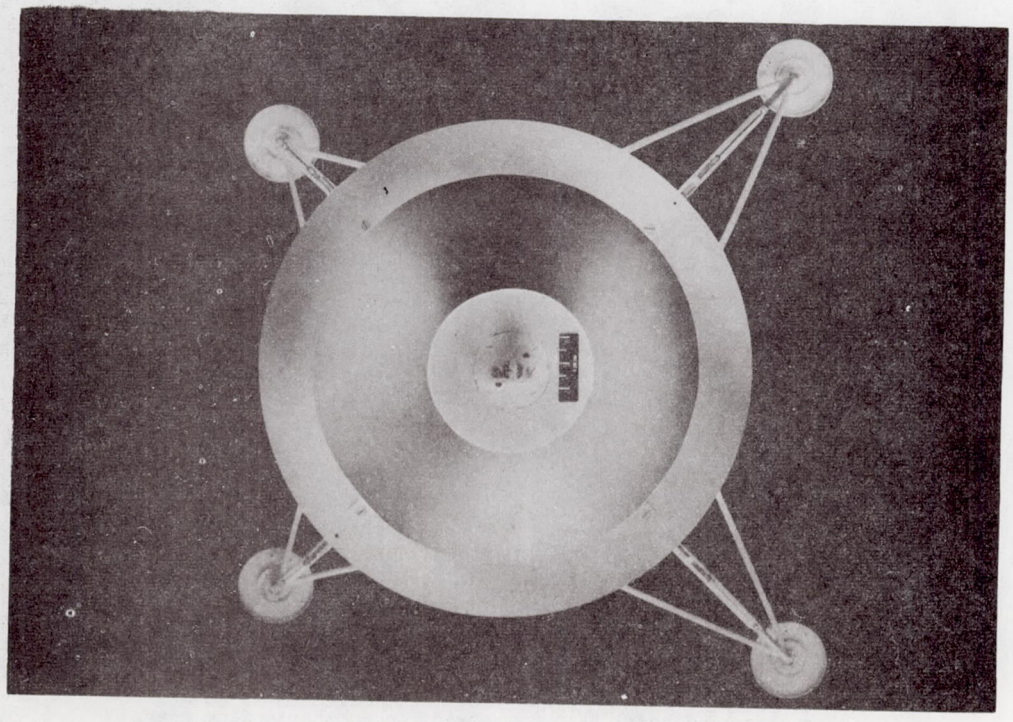

(b) Asymmetric. L-63-555

Figure 3.- Photographs of model showing symmetric and asymmetric four-point landing gears.

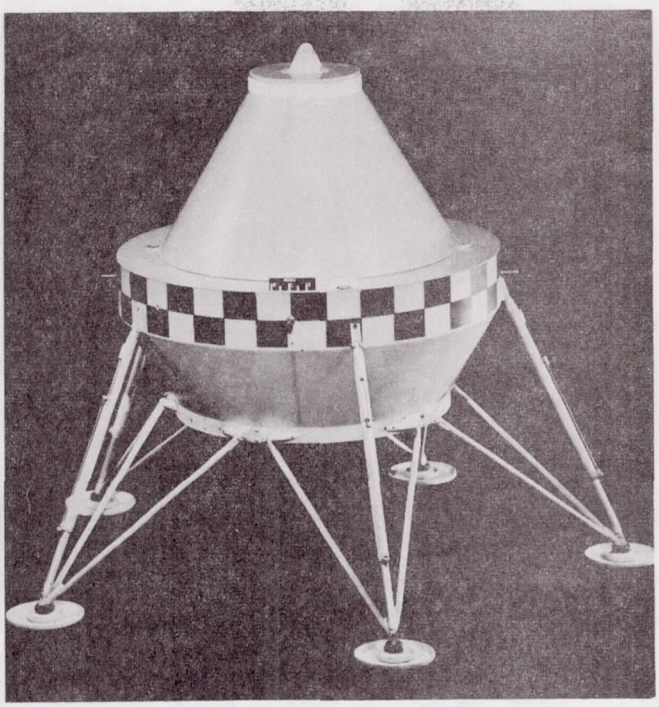

(a) Side view. L-63-1559

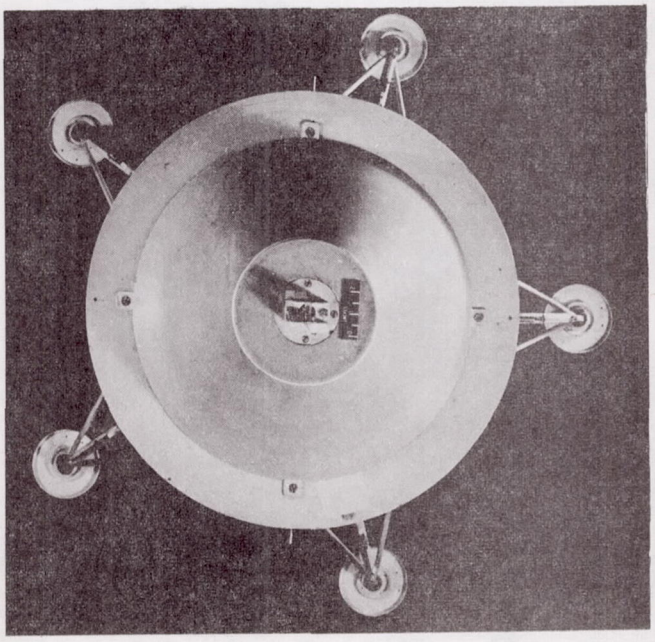

(b) Top view. L-63-1557

Figure 4.- Photograph of model showing symmetric five-point landing gear.

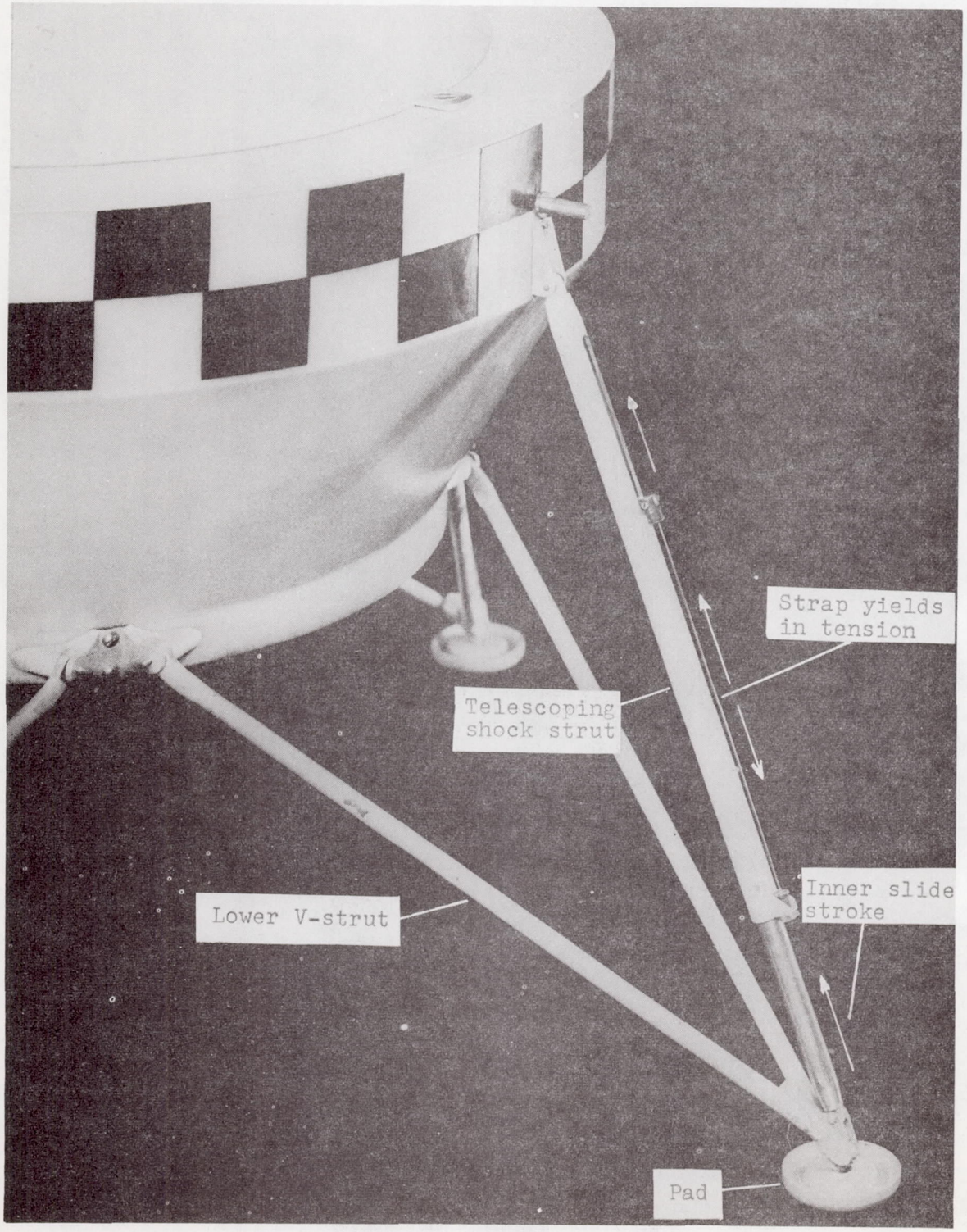

Figure 5.- Landing-gear assembly. L-63-4737

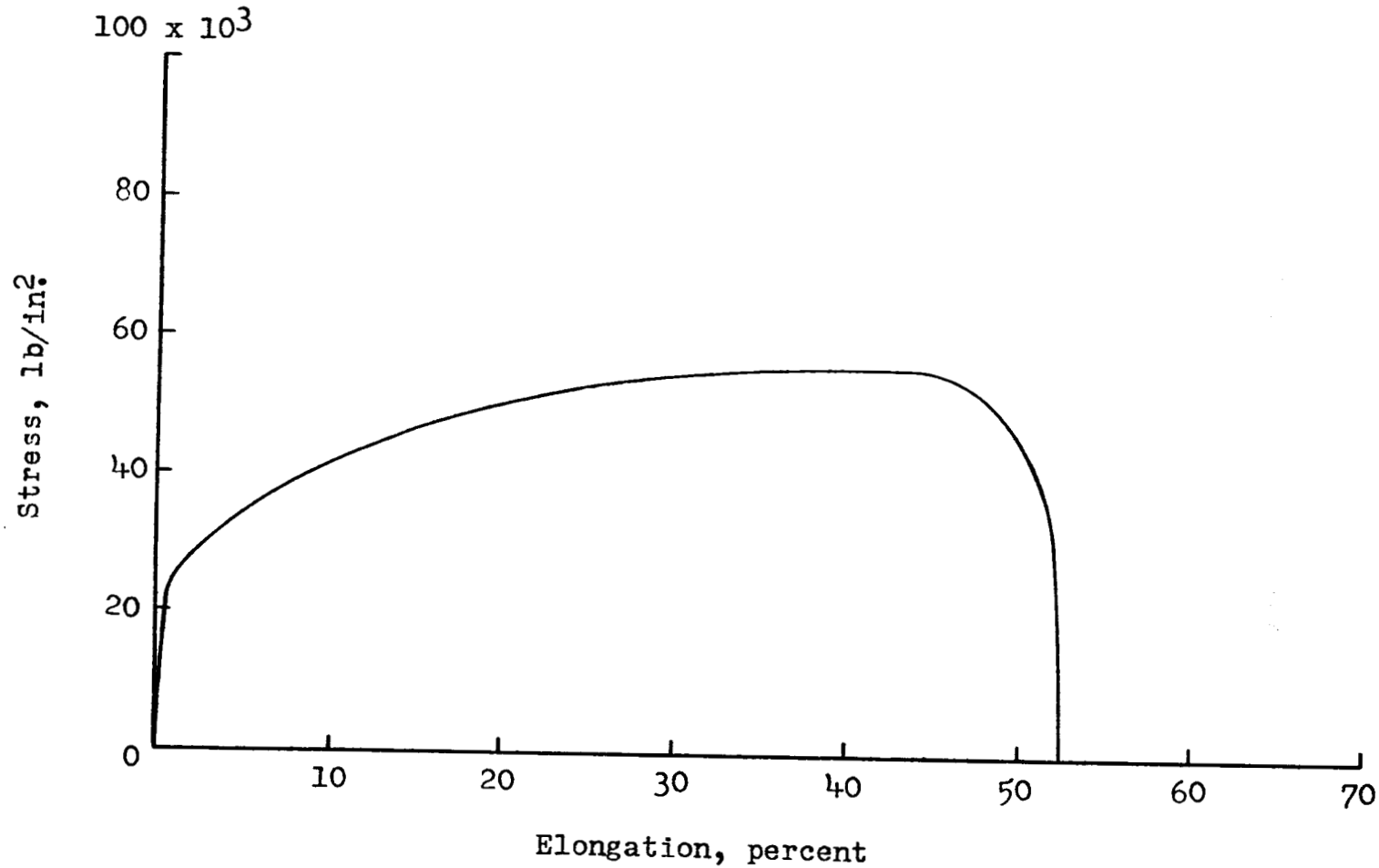

Figure 6.- Stress-strain characteristics of Low-Carbon Nickel metal. Specimen of 0.251-inch diameter annealed 10 minutes at 1,600° F; strain rate, 0.10 in./in./min.

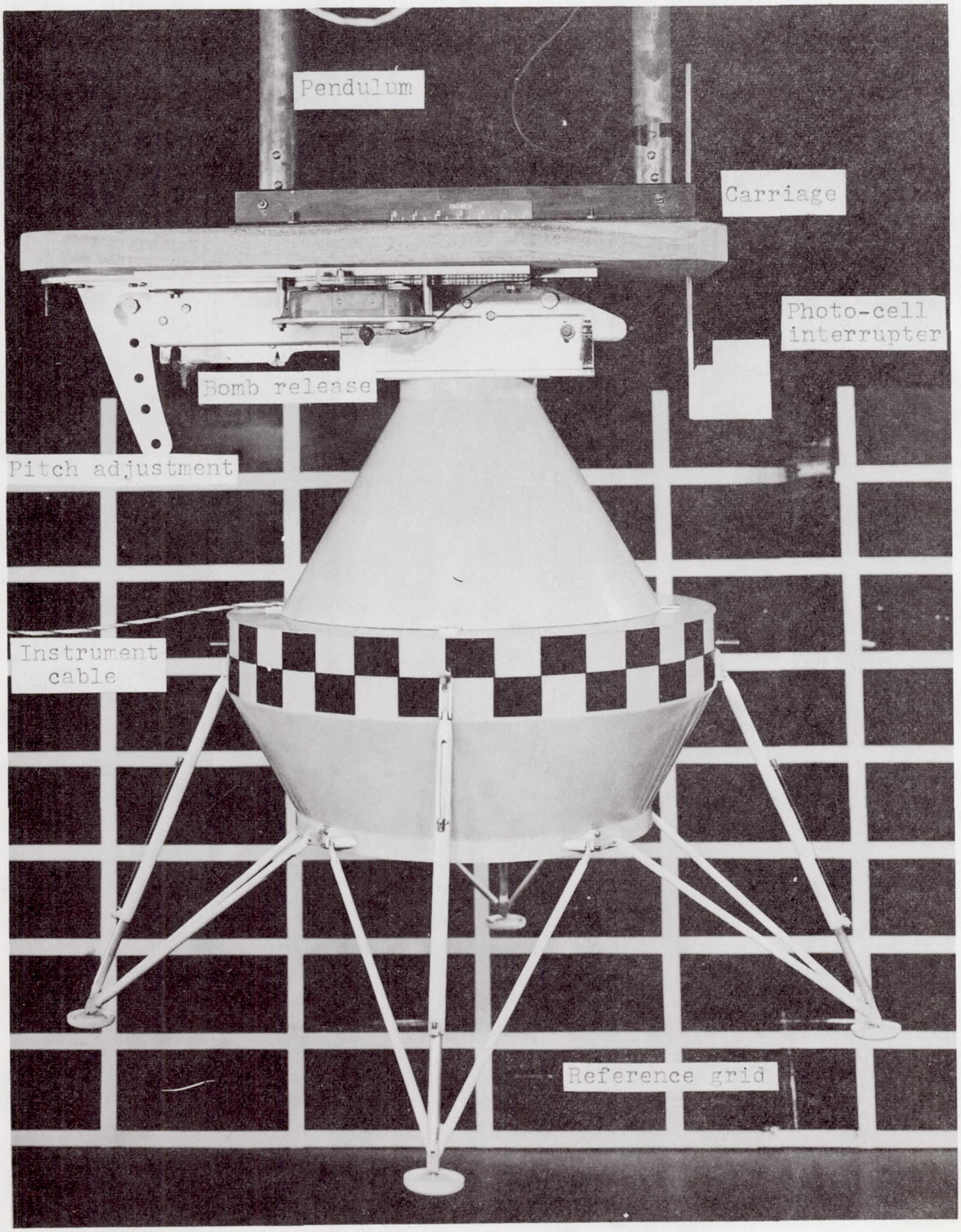

Figure 7.- Model on launching gear. L-62-4270.1

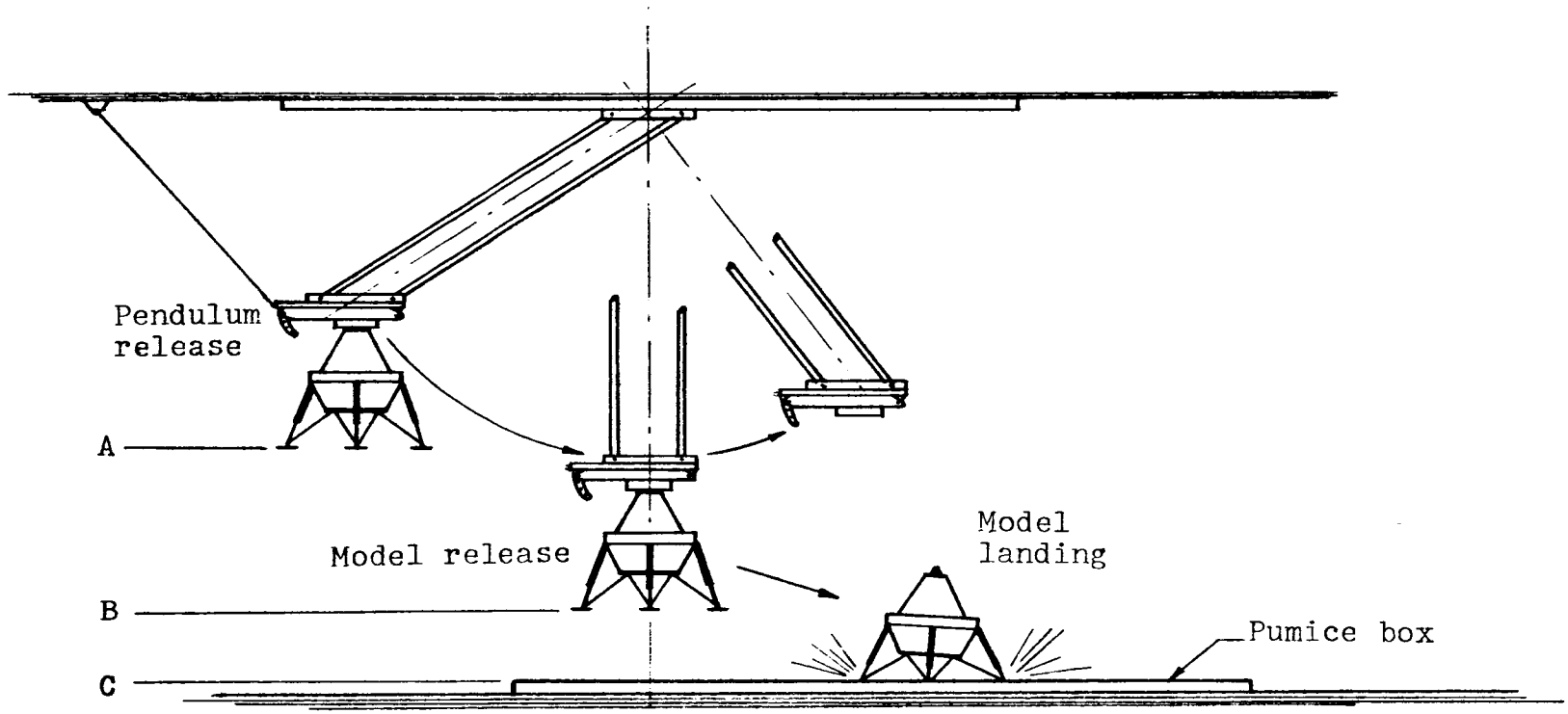

Figure 8.- Sketch showing pendulum operation during model launch and landing.

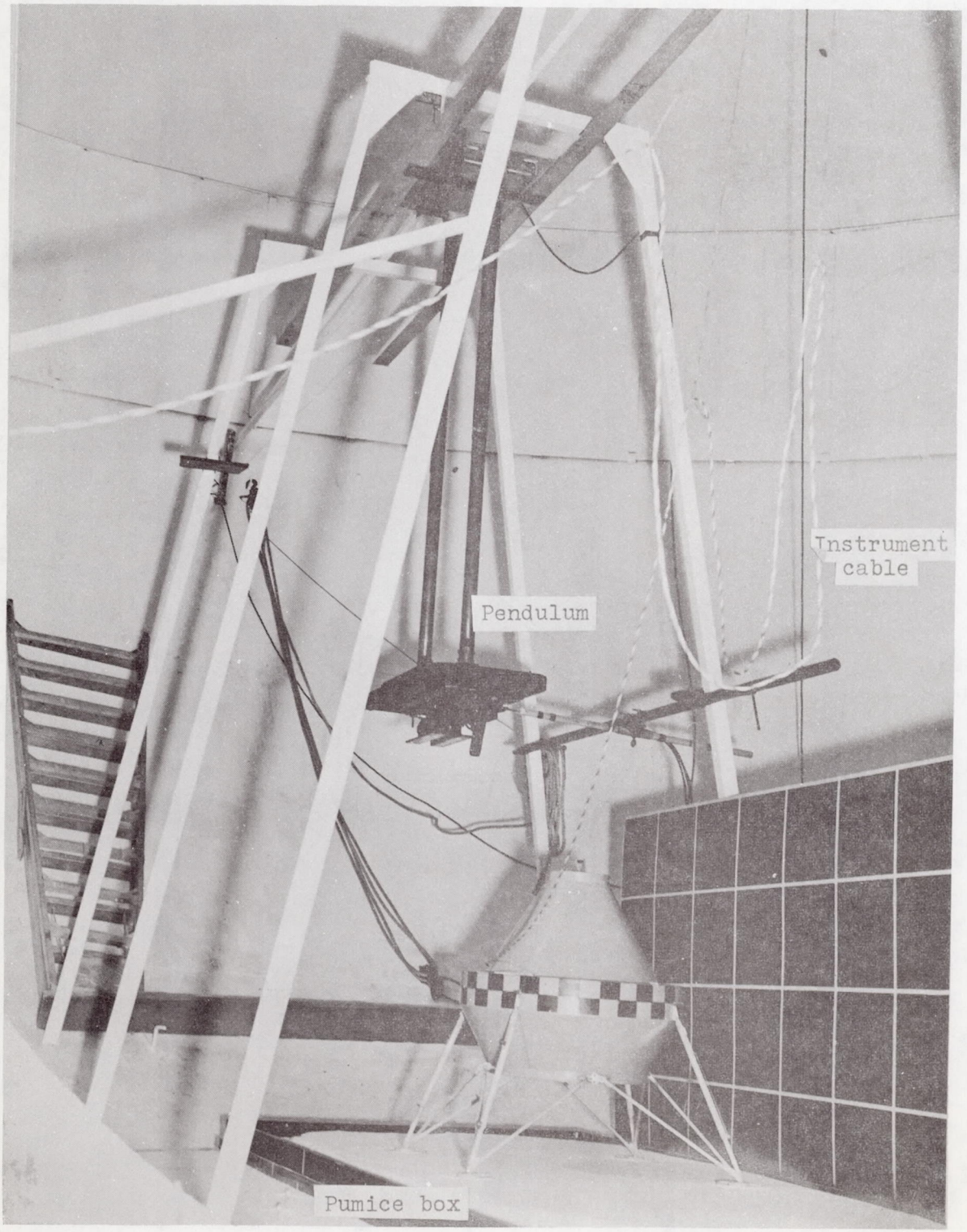

L-62-7386.1

Figure 9.- Model and landing-test apparatus in 41-foot-diameter vacuum sphere.

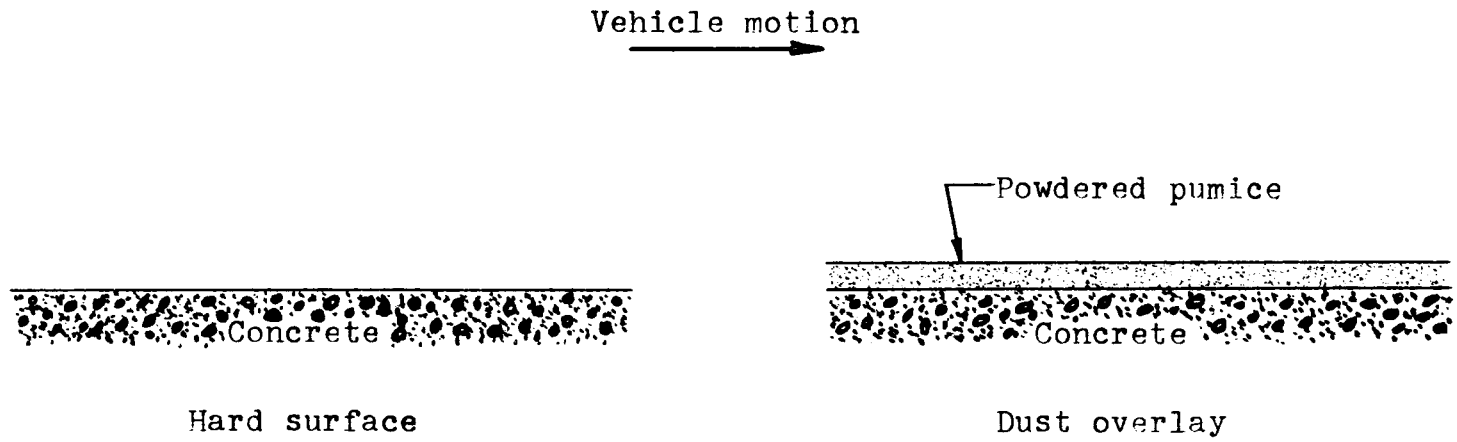

(a) Flat.

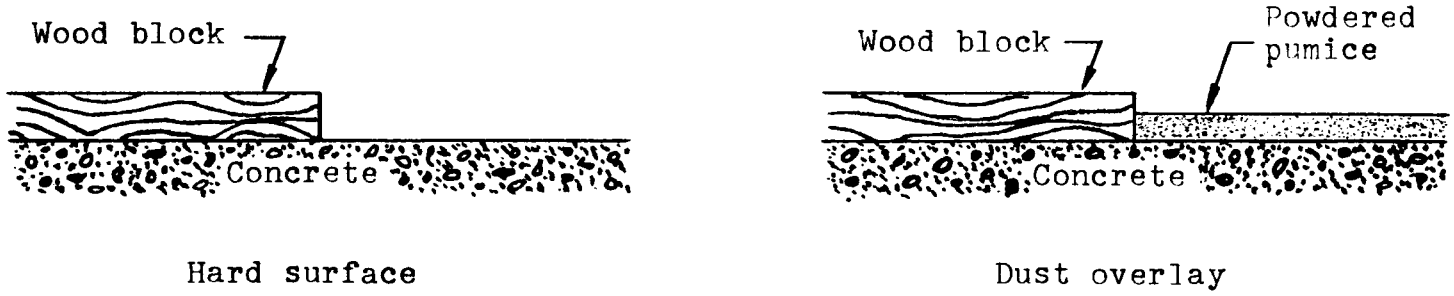

(b) Ledged.

Figure 10.- Sketches illustrating landing-surface topography and materials.

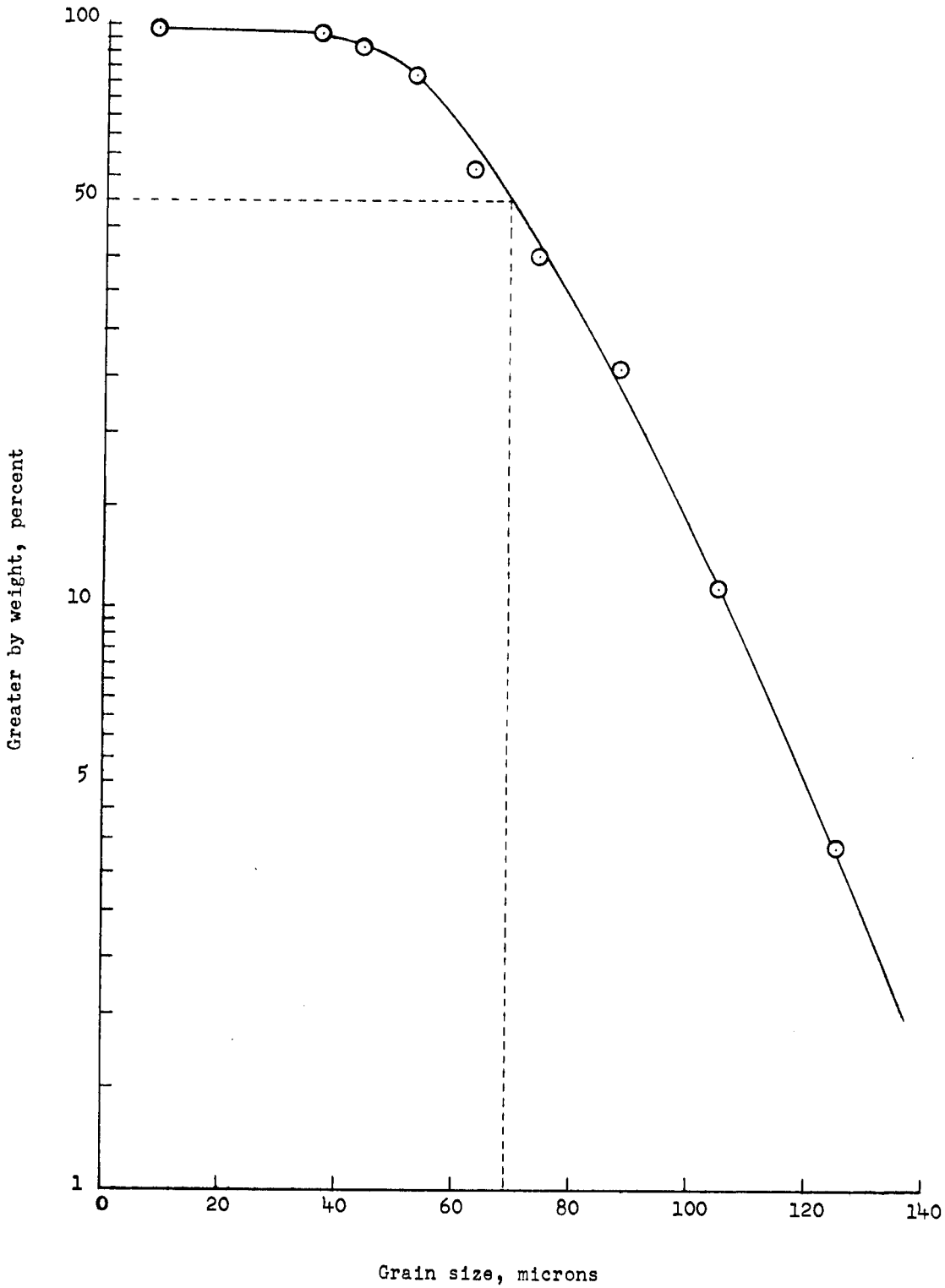

Figure 11.- Grain-size distribution of powdered pumice used for dust overlay.

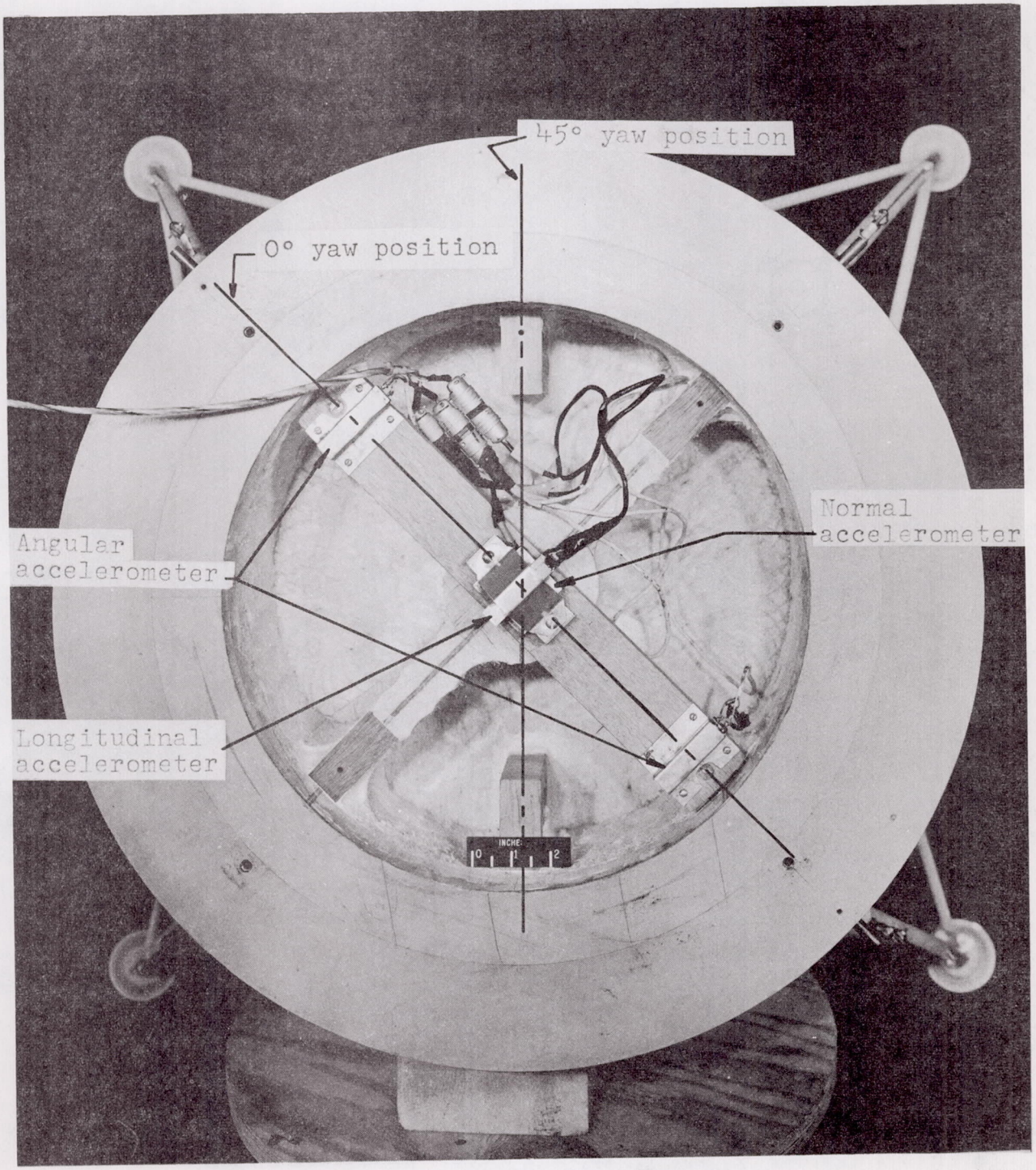

Figure 12.- Instrument installation in model. L-62-4271.1

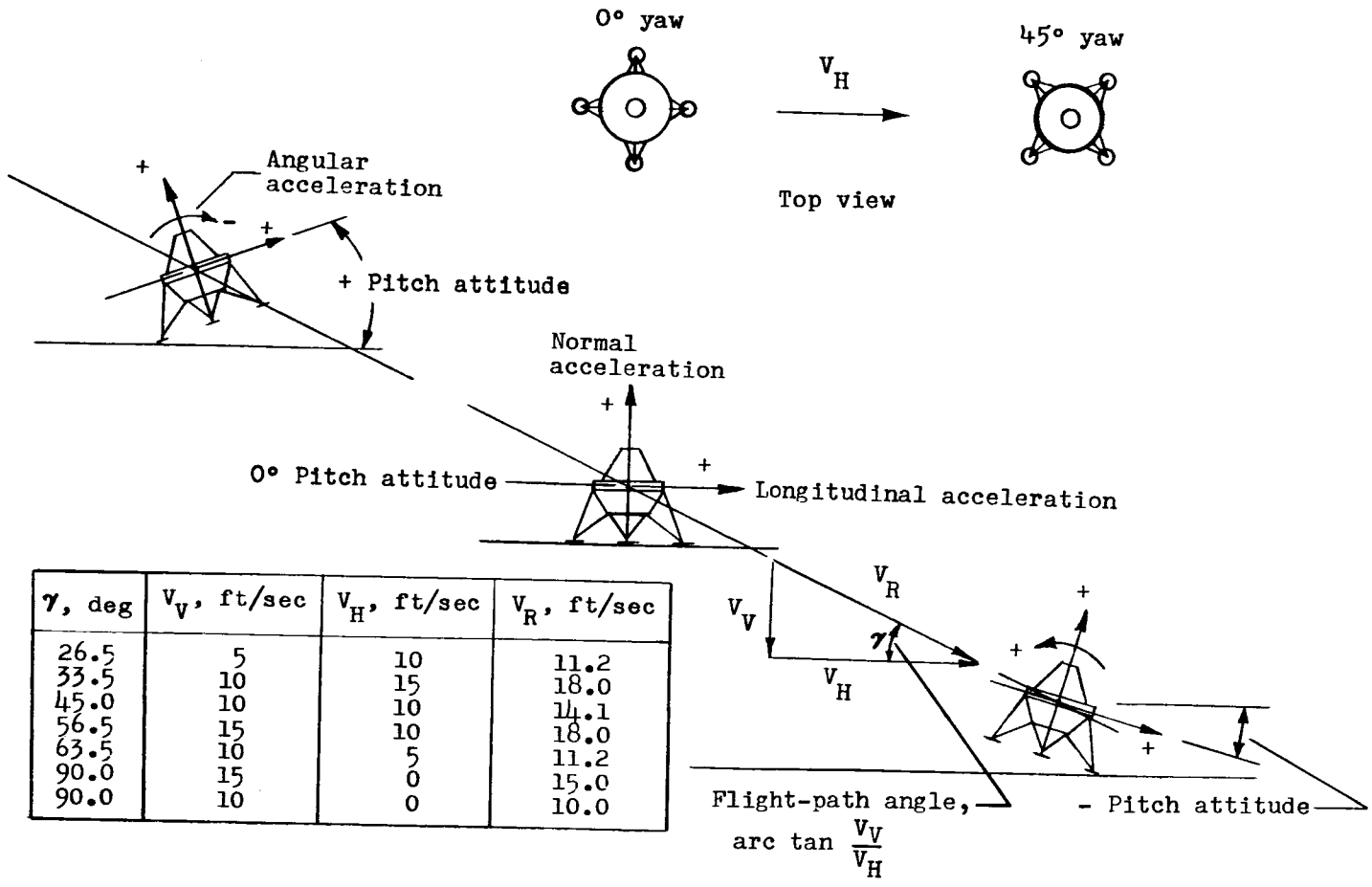

γ, deg	V_V, ft/sec	V_H, ft/sec	V_R, ft/sec
26.5	5	10	11.2
33.5	10	15	18.0
45.0	10	10	14.1
56.5	15	10	18.0
63.5	10	5	11.2
90.0	15	0	15.0
90.0	10	0	10.0

Figure 13.- Sketches identifying acceleration axes, attitudes, flight-path angles, and speeds during landings.

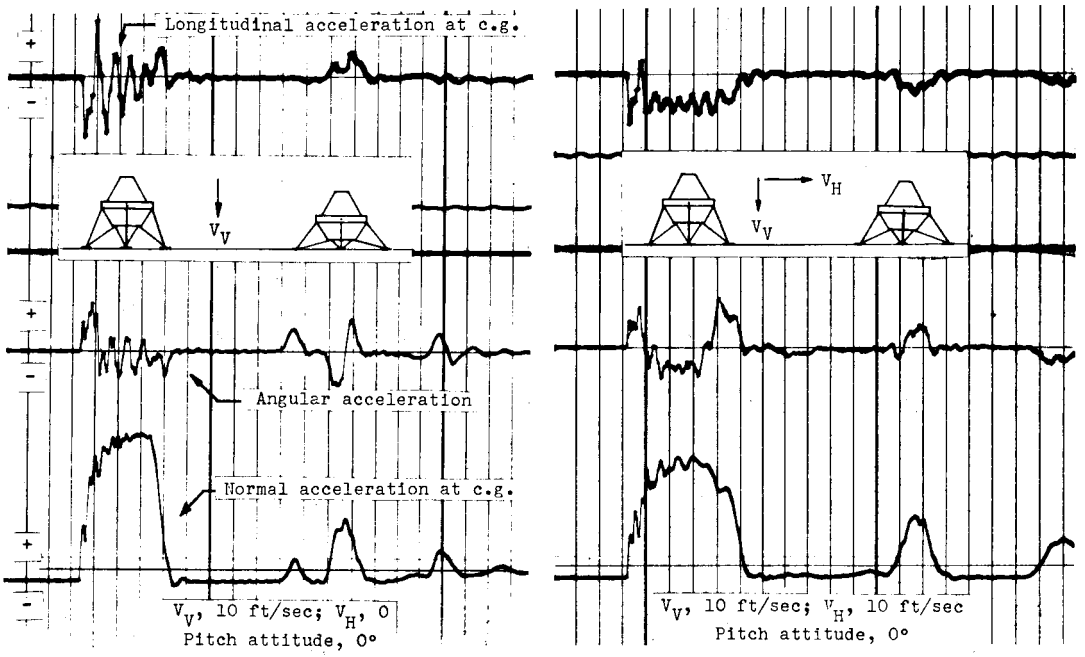

(a) Yaw attitude, 0°.

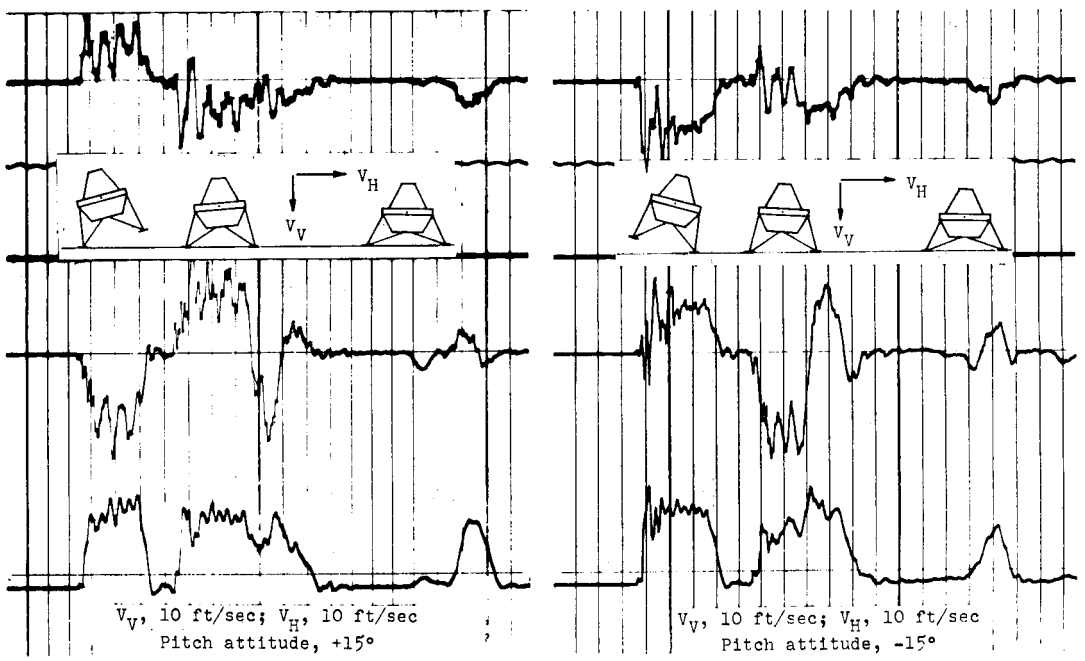

(b) Yaw attitude, 45°.

Figure 14.- Typical oscillograph records of accelerations during landings on flat hard surface at various speeds and attitudes with symmetric four-point landing gear. Roll attitude, 0°.

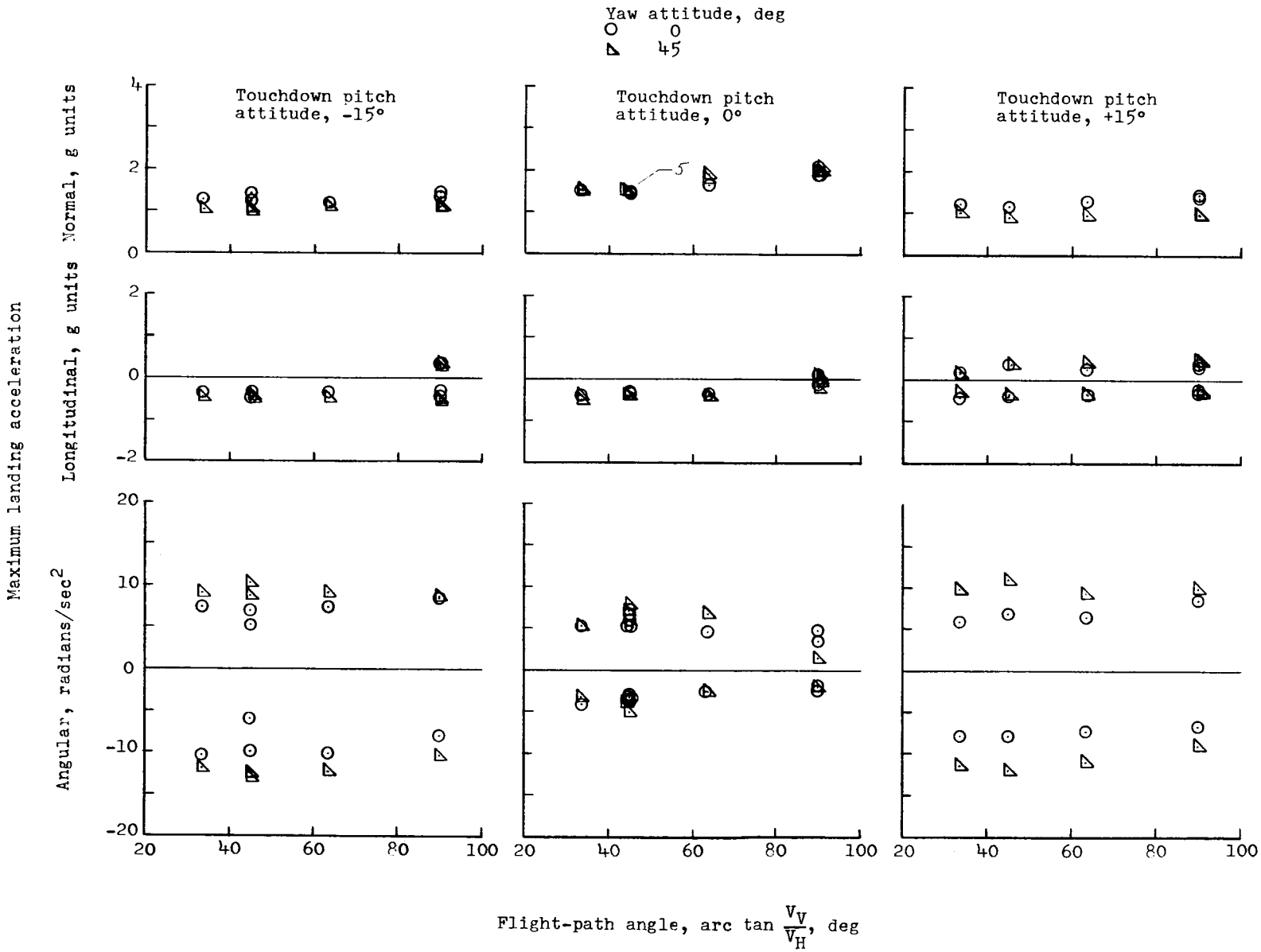

Figure 15.- Effect of flight-path angle on maximum accelerations and stability during landings at various attitudes on flat hard surface with symmetric four-point landing gear. Roll attitude, 0°.

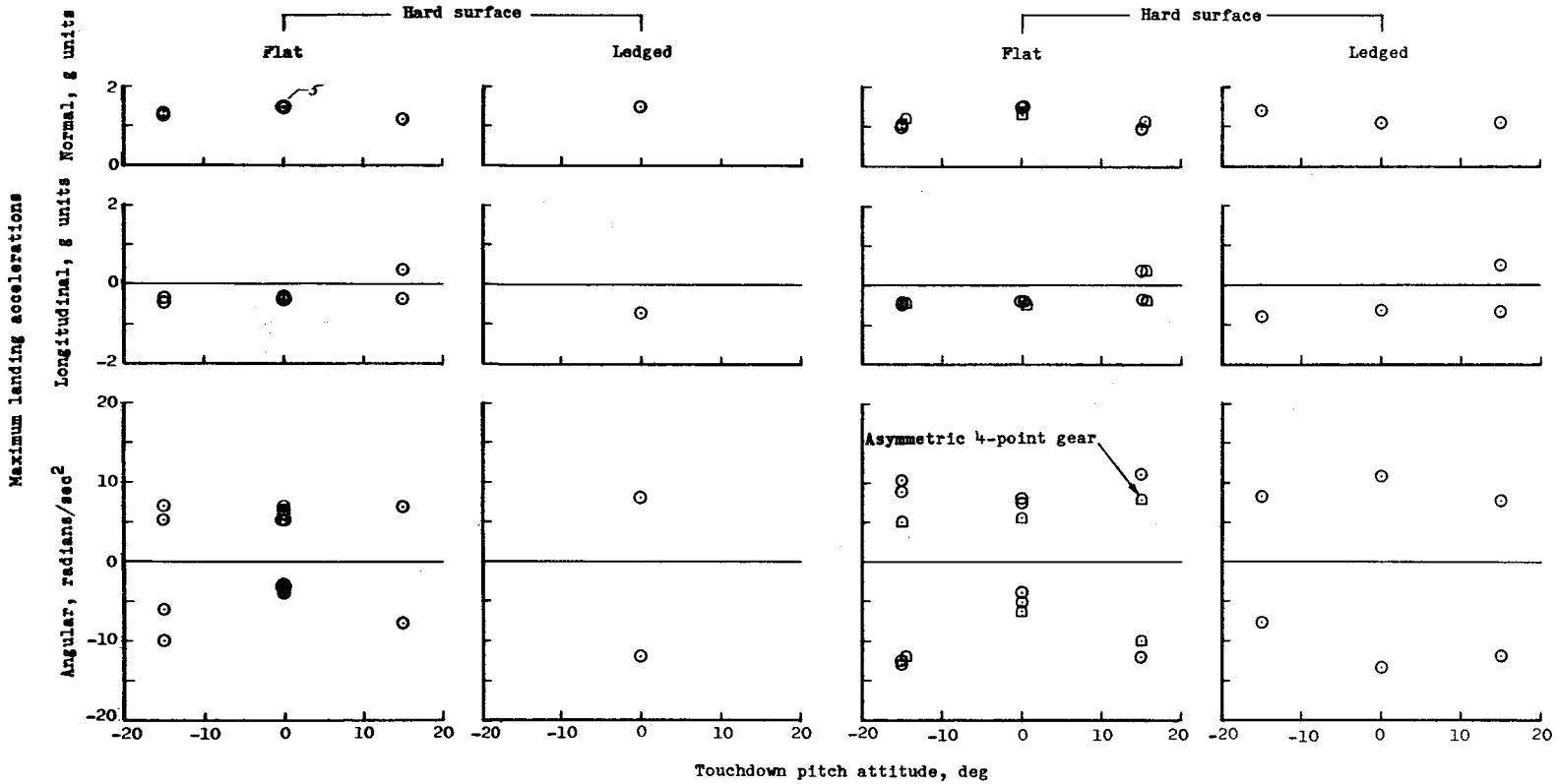

(a) Yaw attitude, 0°.

(b) Yaw attitude, 45°.

Figure 16.- Effect of landing attitude and surface topography on maximum accelerations and stability during landings on hard surface with symmetric four-point landing gear. Roll attitude, 0°; flight-path angle, 45°; V_V, 10 ft/sec; V_H, 10 ft/sec.

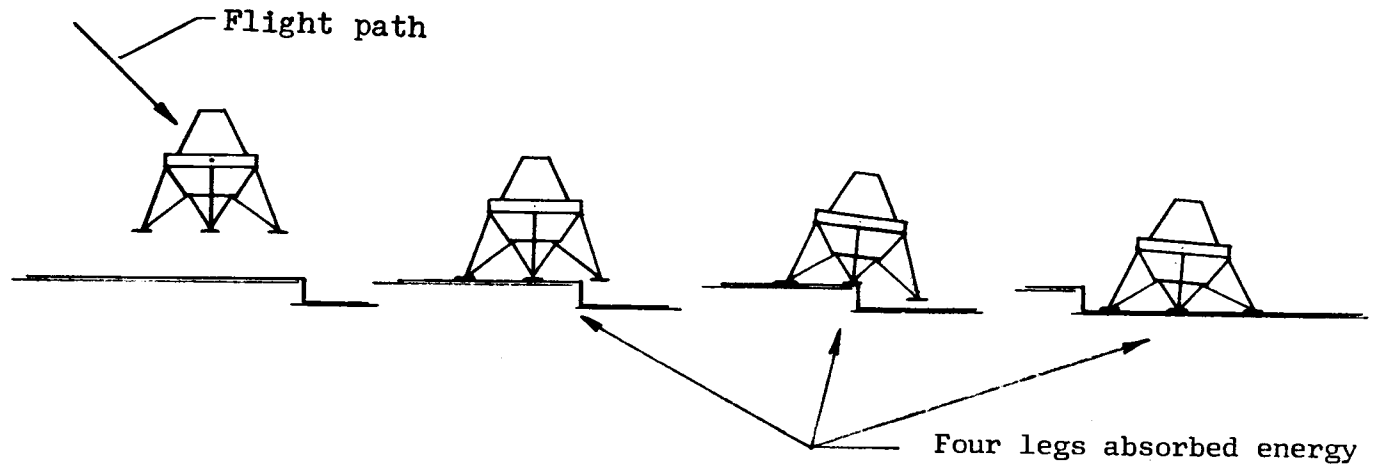

(a) Three-gear initial impact.

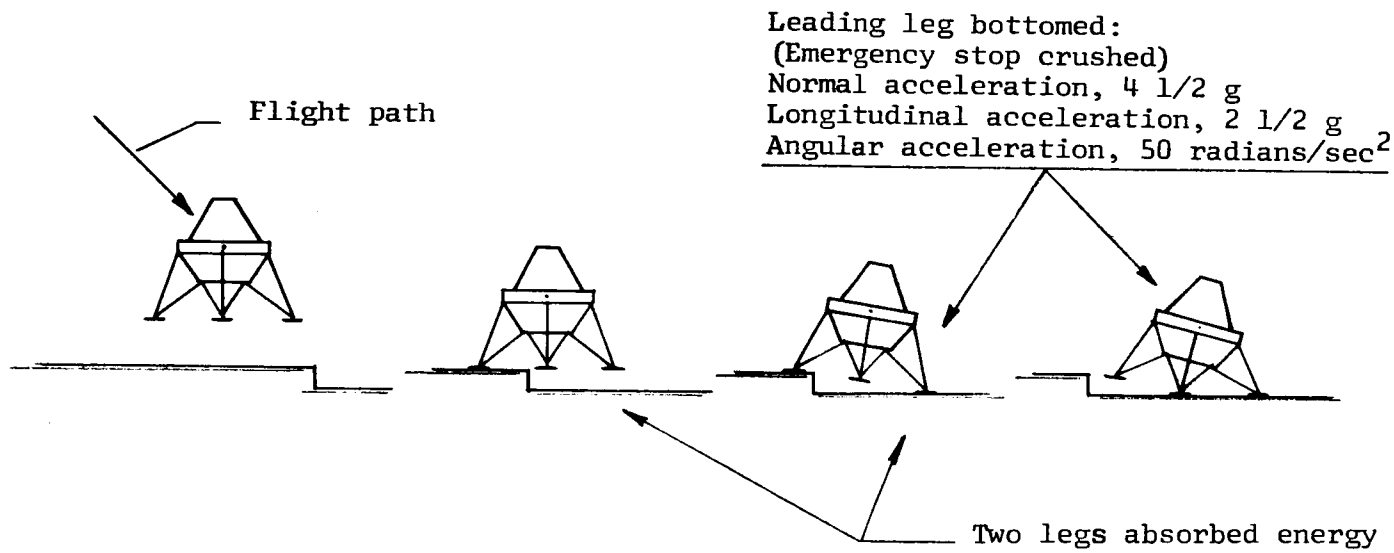

(b) One-gear initial impact.

Figure 17.- Sketches showing sequence of two landing conditions on ledged hard surface with symmetric four-point landing gear. Roll attitude, 0°; pitch attitude, 0°; yaw attitude, 0°; flight-path angle, 45°; V_V, 10 ft/sec; V_H, 10 ft/sec.

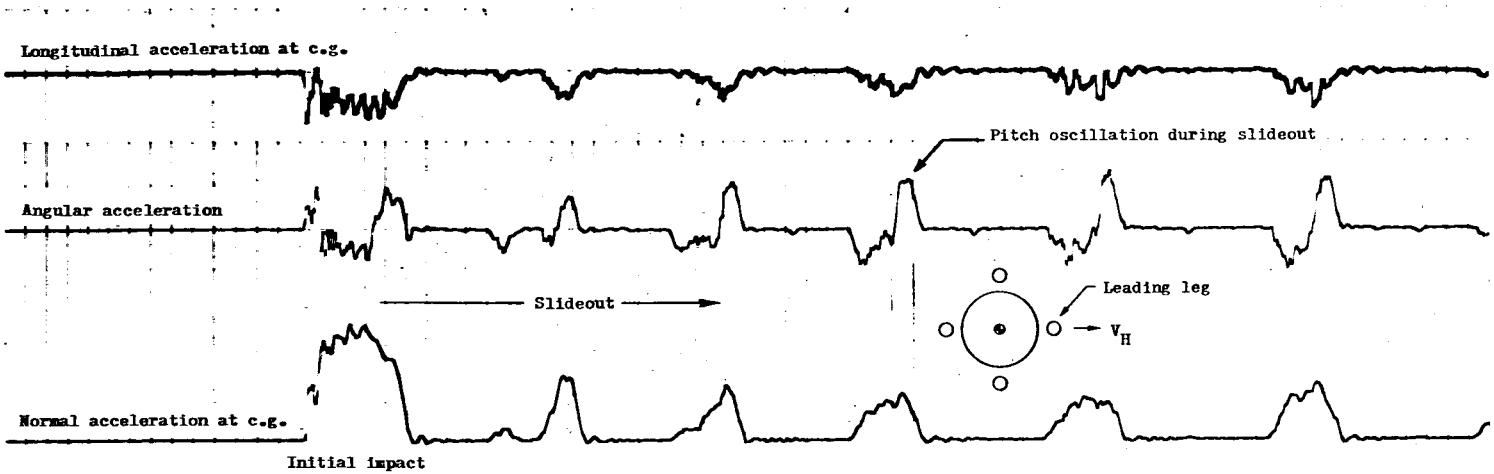

(a) Yaw attitude, 0°.

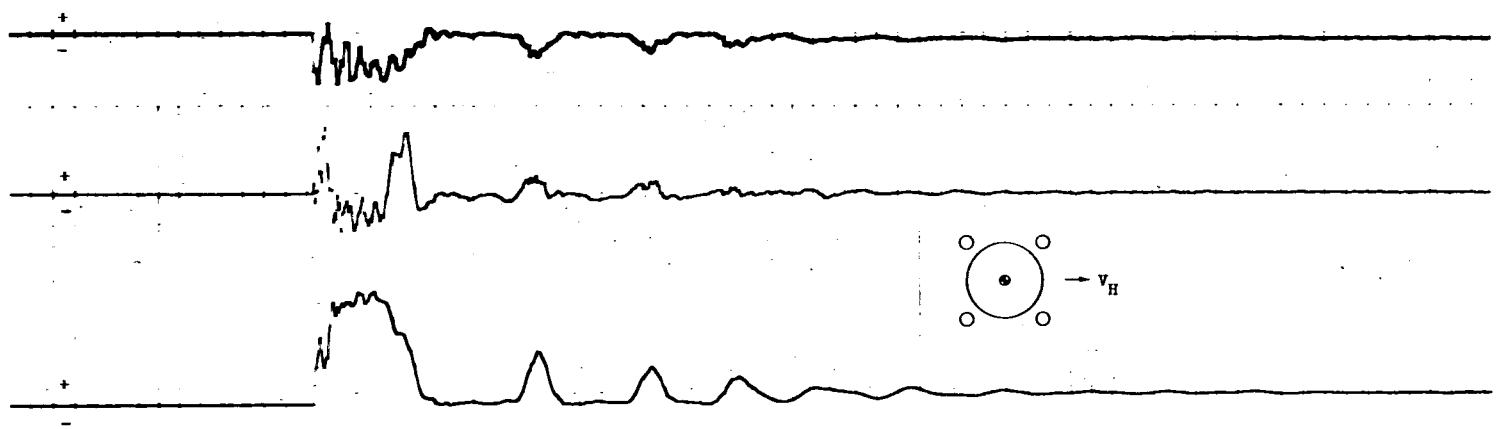

(b) Yaw attitude, 45°.

Figure 18.- Typical oscillograph records of accelerations during landing impact and slideout on flat hard surface at 0° and 45° yaw attitudes with symmetric four-point landing gear. Pitch attitude, 0°; roll attitude, 0°; flight-path angle, 45°; V_V, 10 ft/sec; V_H, 10 ft/sec.

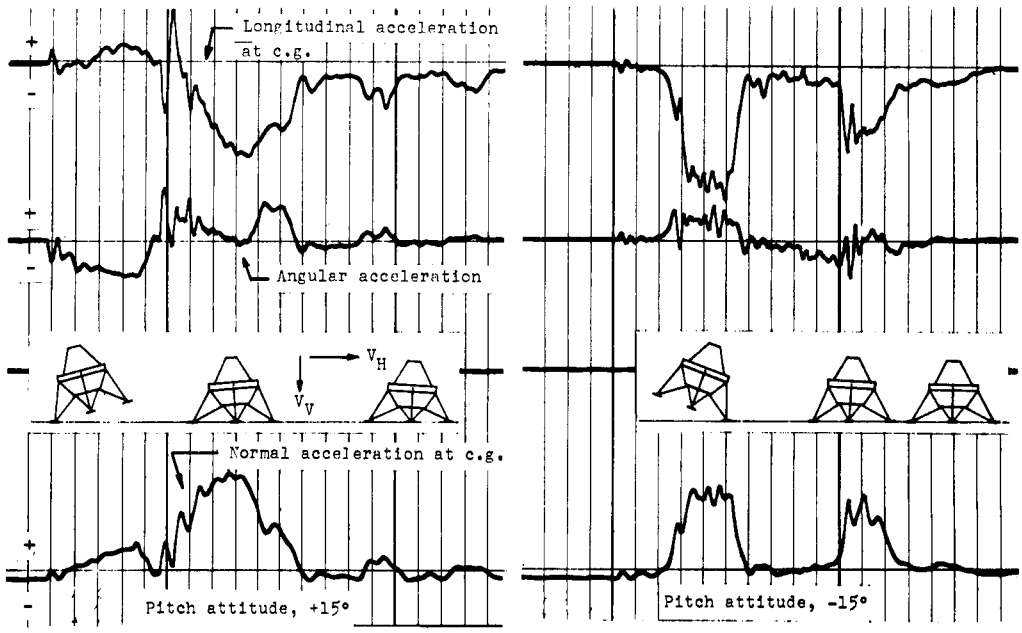

(a) Yaw attitude, 0°.

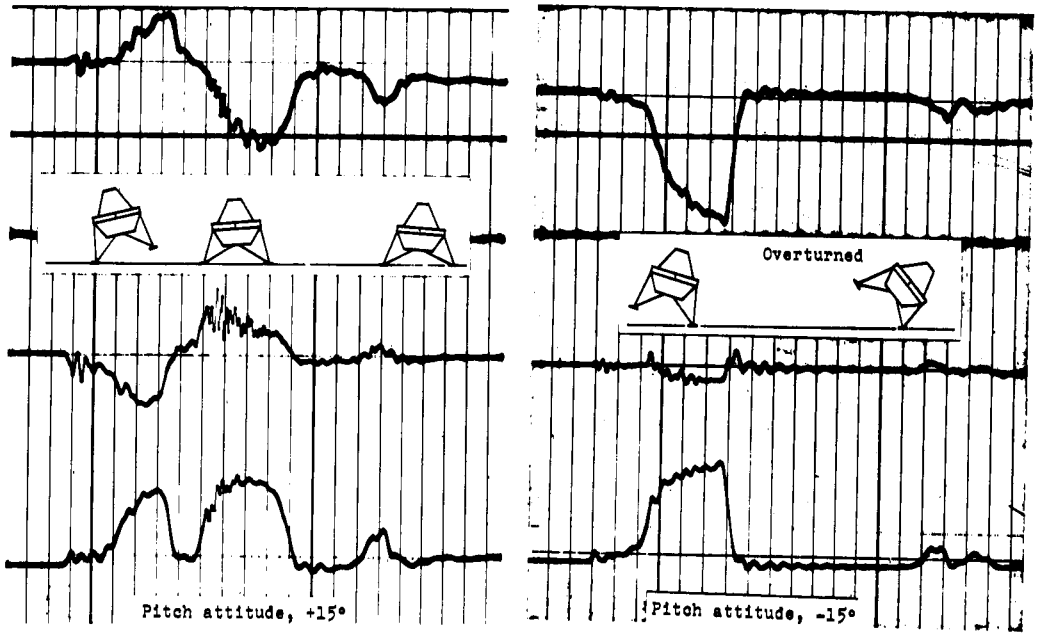

(b) Yaw attitude, 45°.

Figure 19.- Typical oscillograph records of accelerations during landings on flat dust overlay at various attitudes with symmetric four-point landing gear. Flight-path angle, 45°; V_V, 10 ft/sec; V_H, 10 ft/sec; roll attitude, 0°; depth of dust, 21 inches.

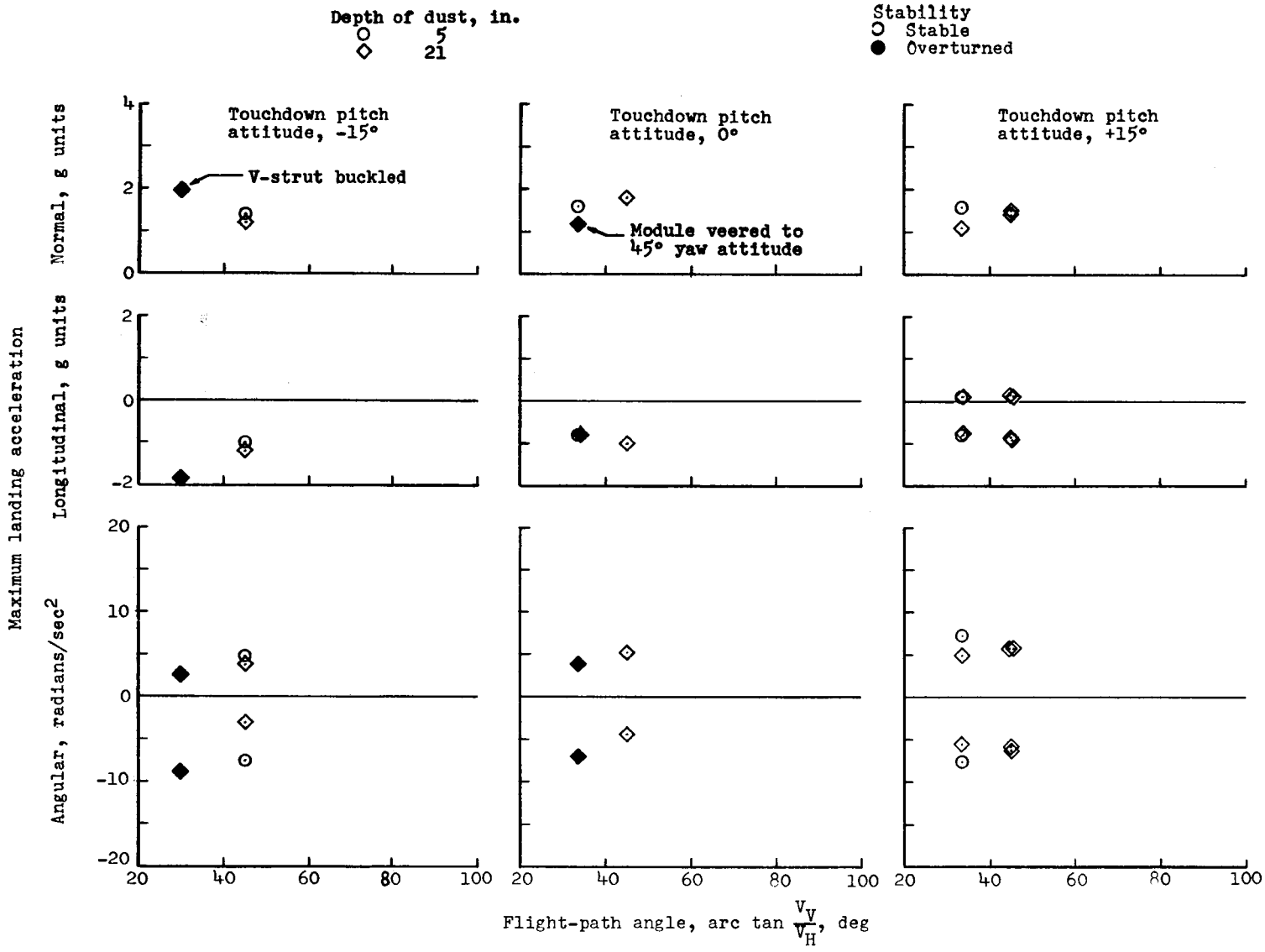

(a) Yaw attitude, 0°.

Figure 20.- Effect of flight-path angle on maximum accelerations and stability during landings at various attitudes on flat dust overlay with symmetric four-point landing gear. Roll attitude, 0°.

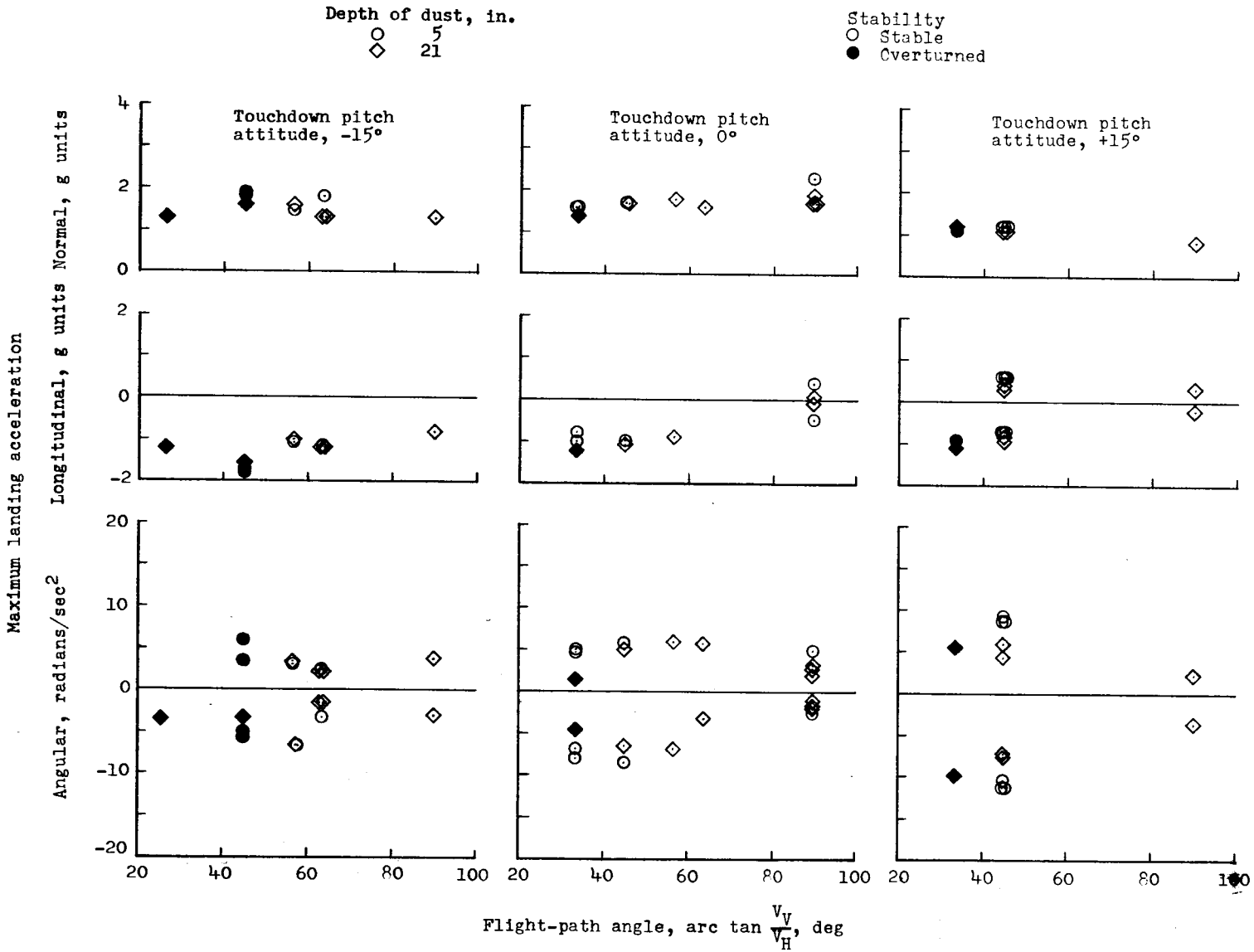

(b) Yaw attitude, 45°.

Figure 20.- Concluded.

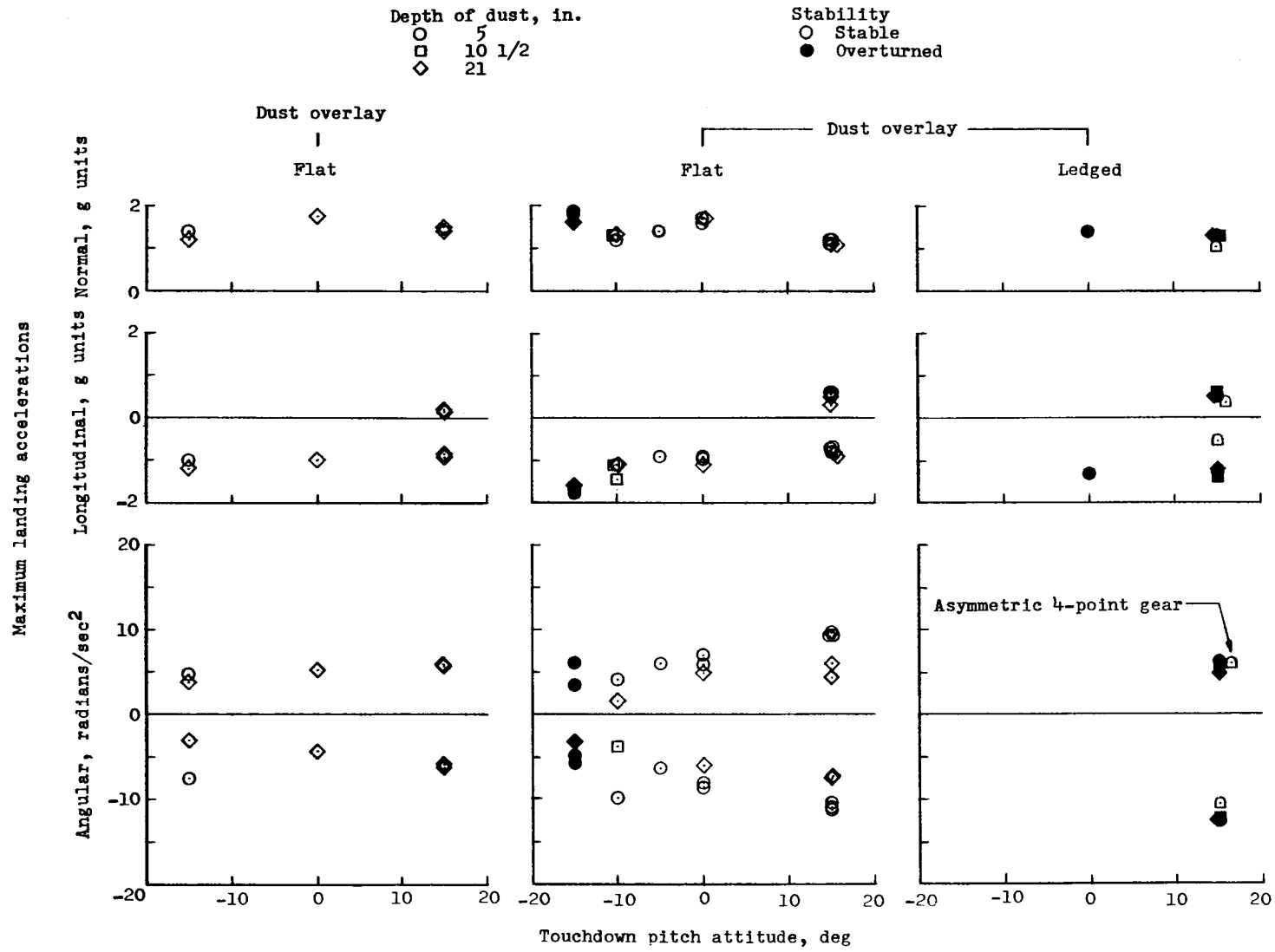

(a) Yaw attitude, 0°.

(b) Yaw attitude, 45°.

Figure 21.- Effect of landing attitude and surface topography on maximum accelerations and stability during landings on dust overlay with symmetric four-point landing gear. Roll attitude, 0°; flight-path angle, 45°; V_V, 10 ft/sec; V_H, 10 ft/sec.

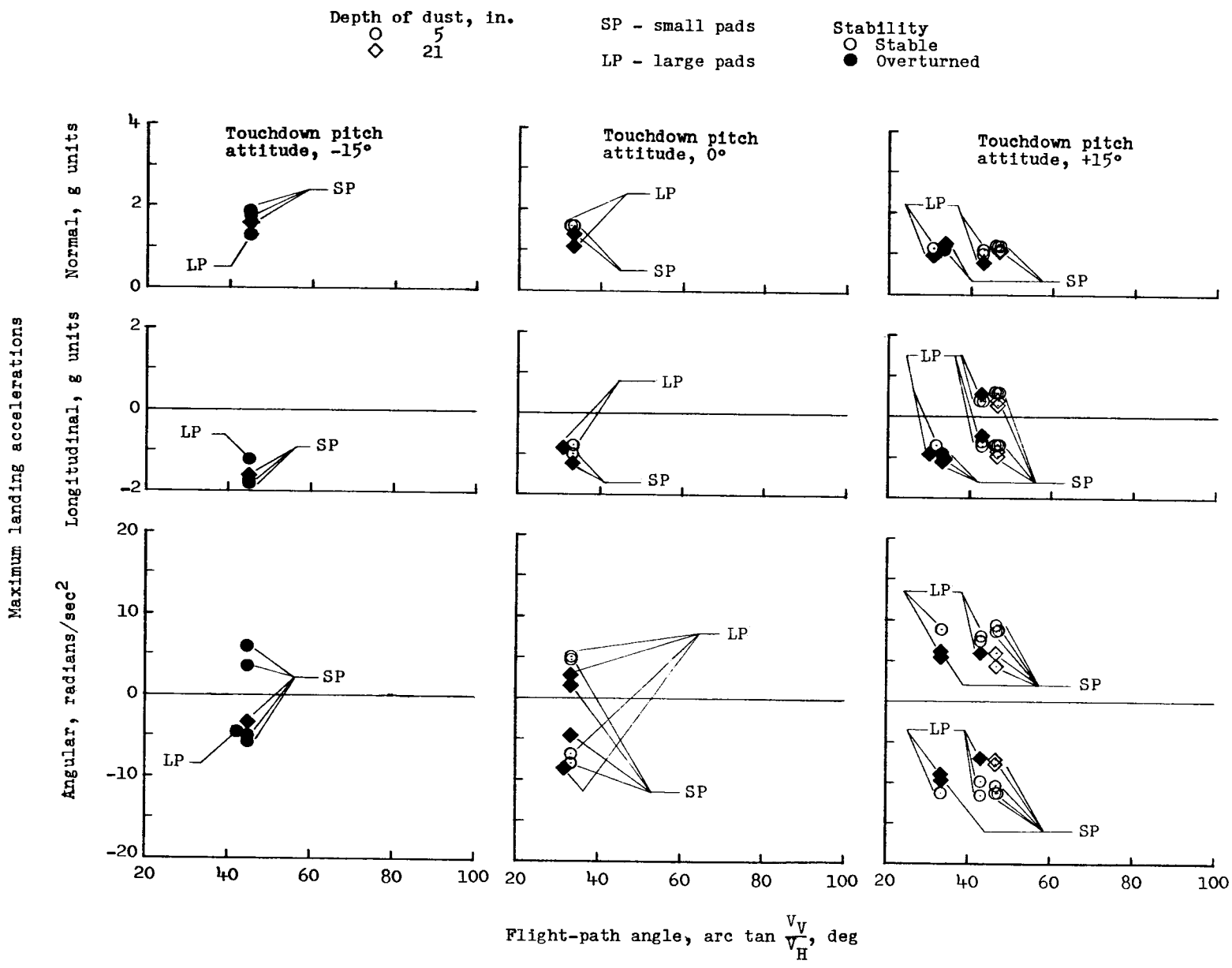

Figure 22.- Effect of depth of dust overlay and pad size on landing stability for various landing conditions. Roll attitude, 0°; yaw attitude, 45°; symmetric four-point landing gear.

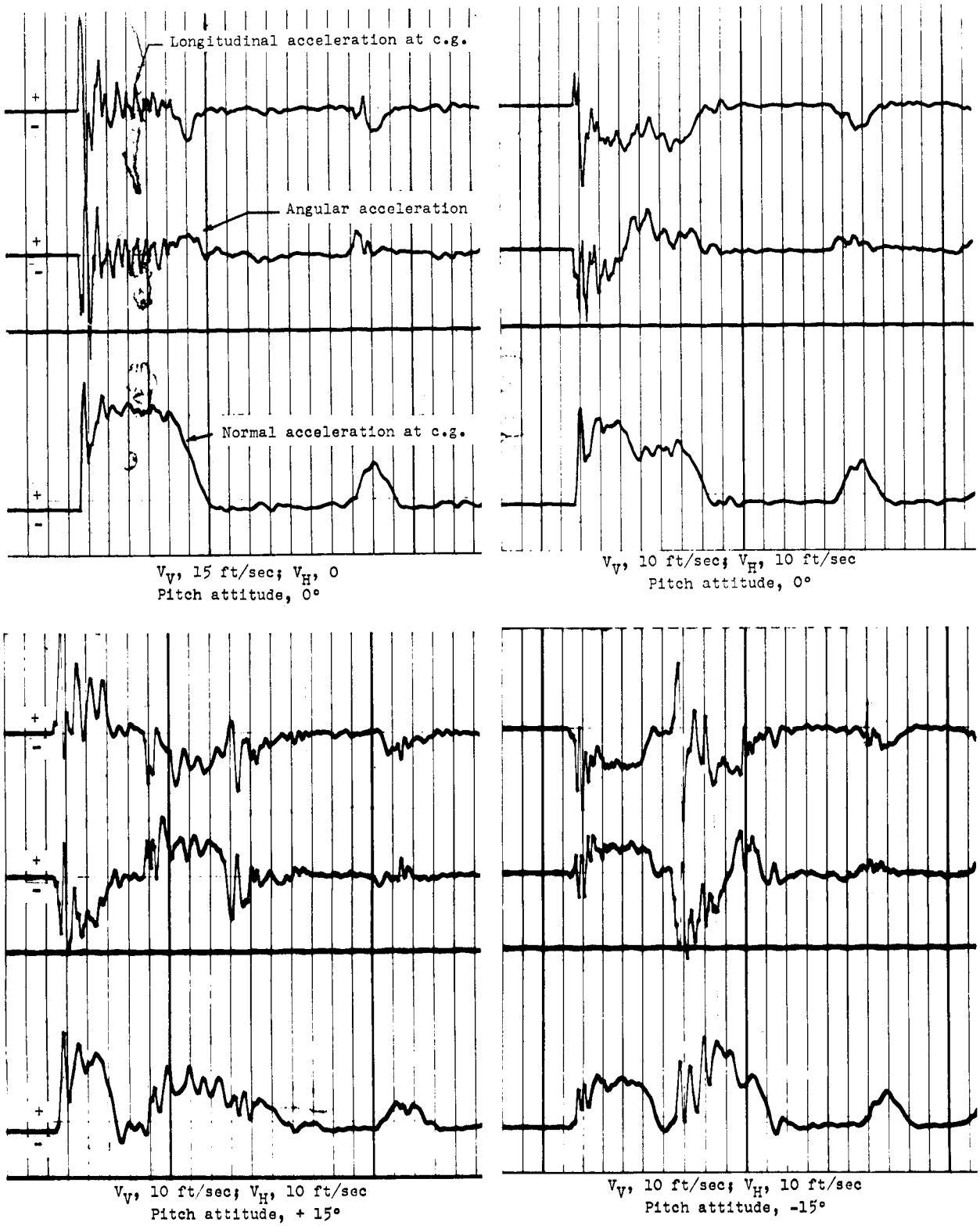

V_V, 15 ft/sec; V_H, 0
Pitch attitude, 0°

V_V, 10 ft/sec; V_H, 10 ft/sec
Pitch attitude, 0°

V_V, 10 ft/sec; V_H, 10 ft/sec
Pitch attitude, + 15°

V_V, 10 ft/sec; V_H, 10 ft/sec
Pitch attitude, -15°

Figure 23.- Typical oscillograph records of accelerations during landings on flat hard surface at various speeds and attitudes with asymmetric four-point landing gear. Yaw attitude, 45°; roll attitude, 0°.

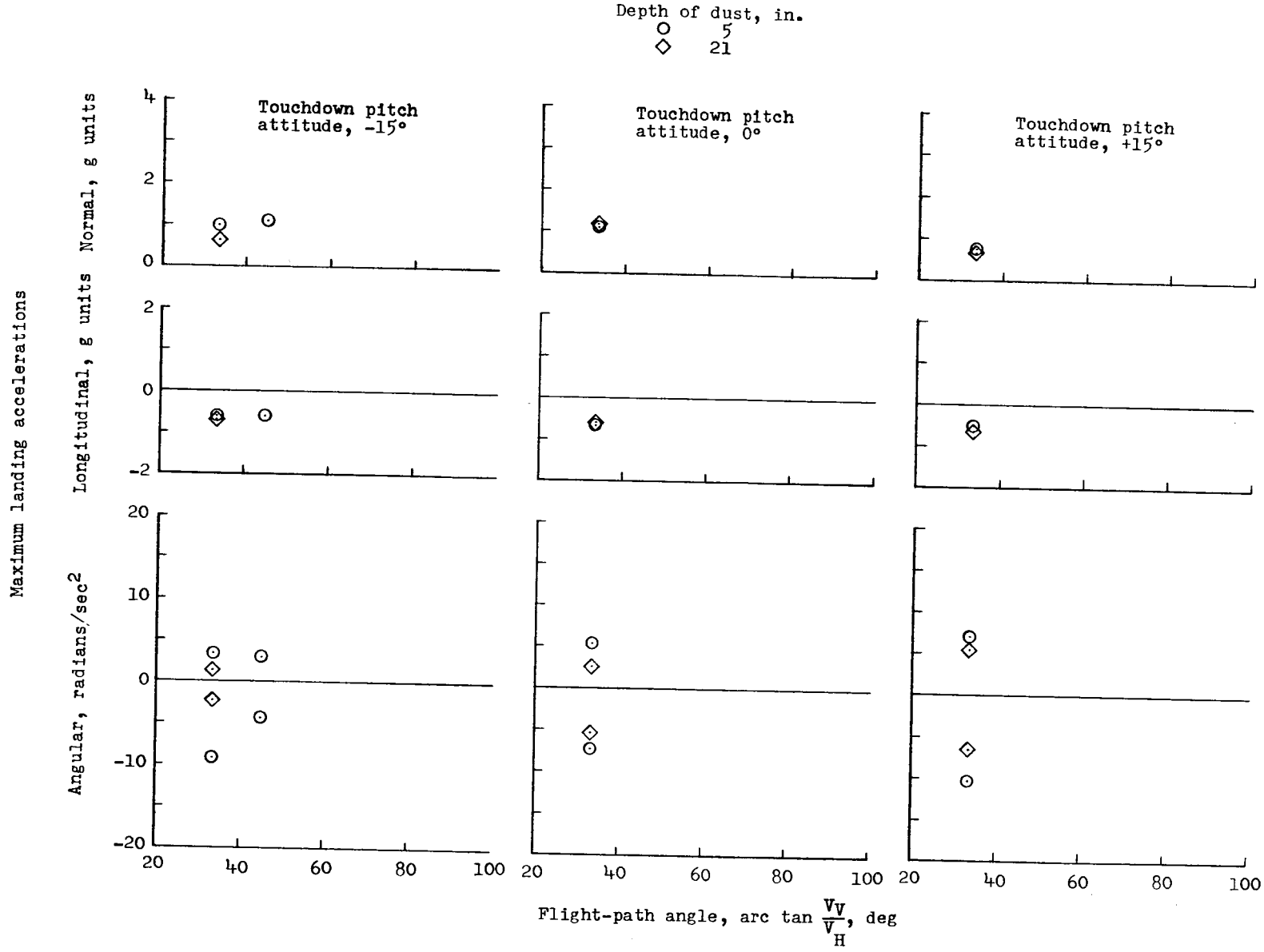

Figure 24.- Effect of asymmetric four-point landing gear on maximum accelerations and stability for various landing conditions on flat dust overlay. Roll attitude, 0°; yaw attitude, 45°.

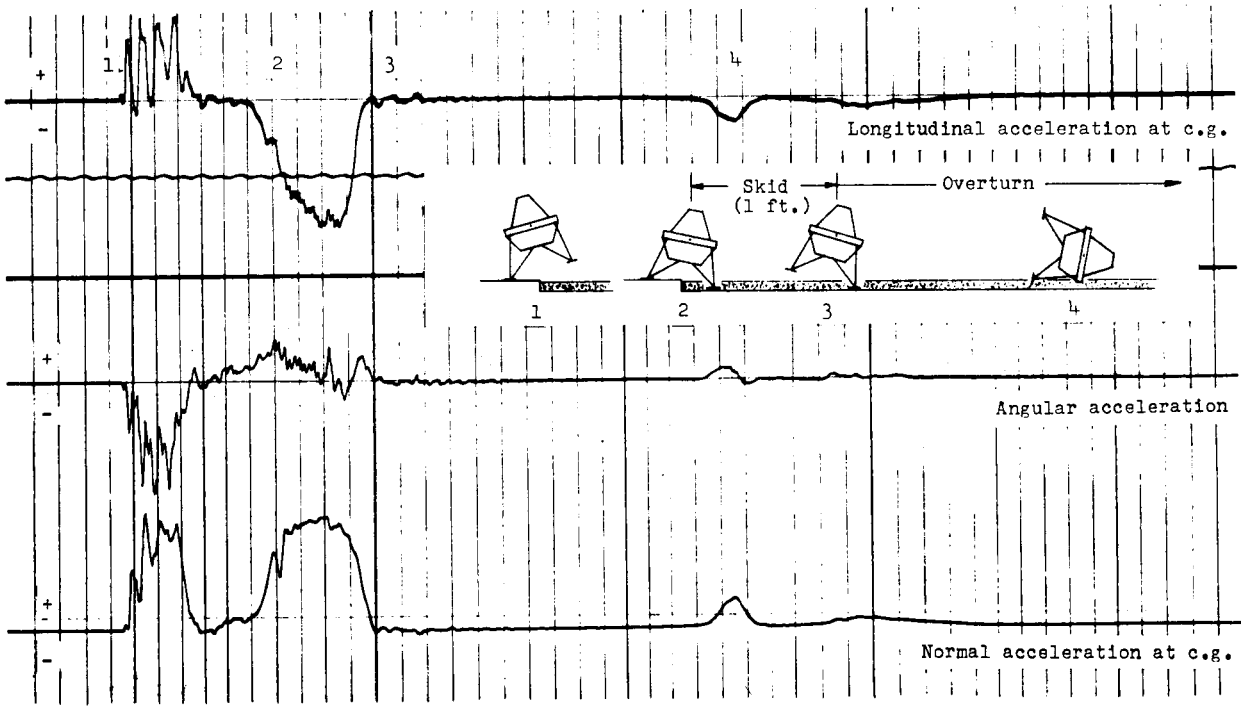

(a) Symmetric four-point gear.

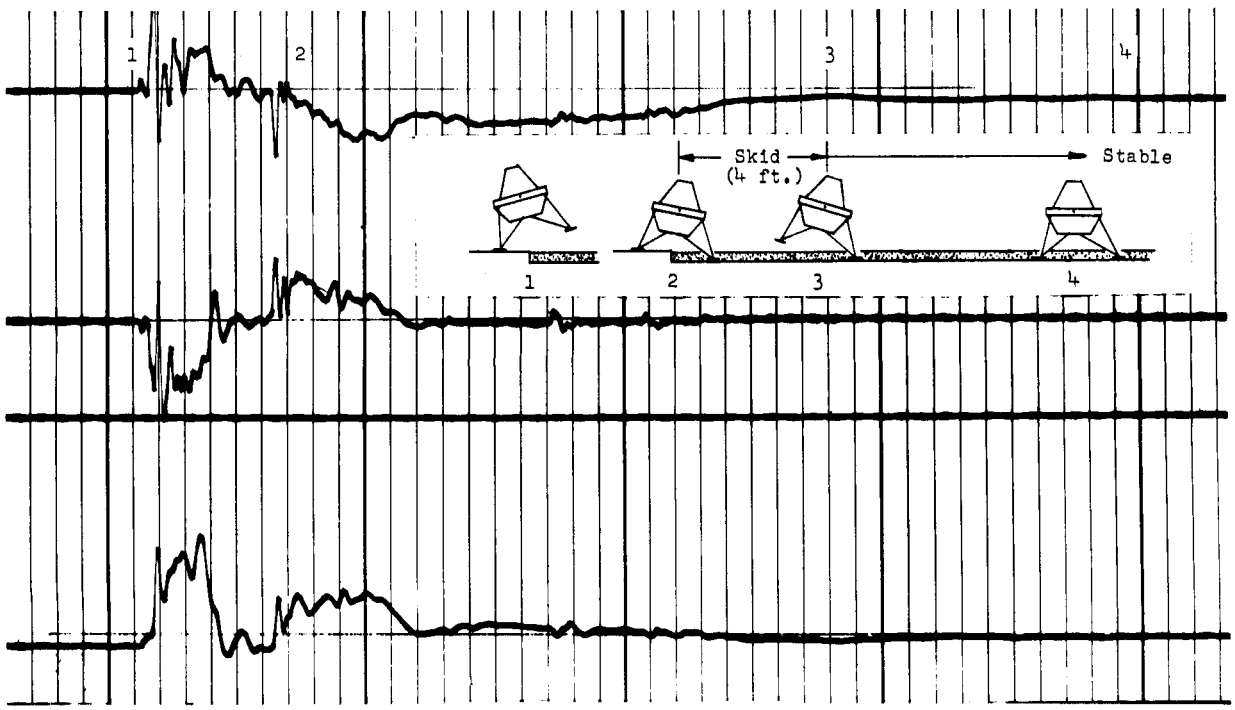

(b) Asymmetric four-point gear.

Figure 25.- Typical oscillograph records of accelerations during landings on ledged surface and dust overlay with symmetric and asymmetric four-point landing gears. Pitch attitude, +15°; roll attitude, 0°; yaw attitude, 45°; flight-path angle, 45°; V_V, 10 ft/sec; V_H, 10 ft/sec; depth of dust, 21 inches.

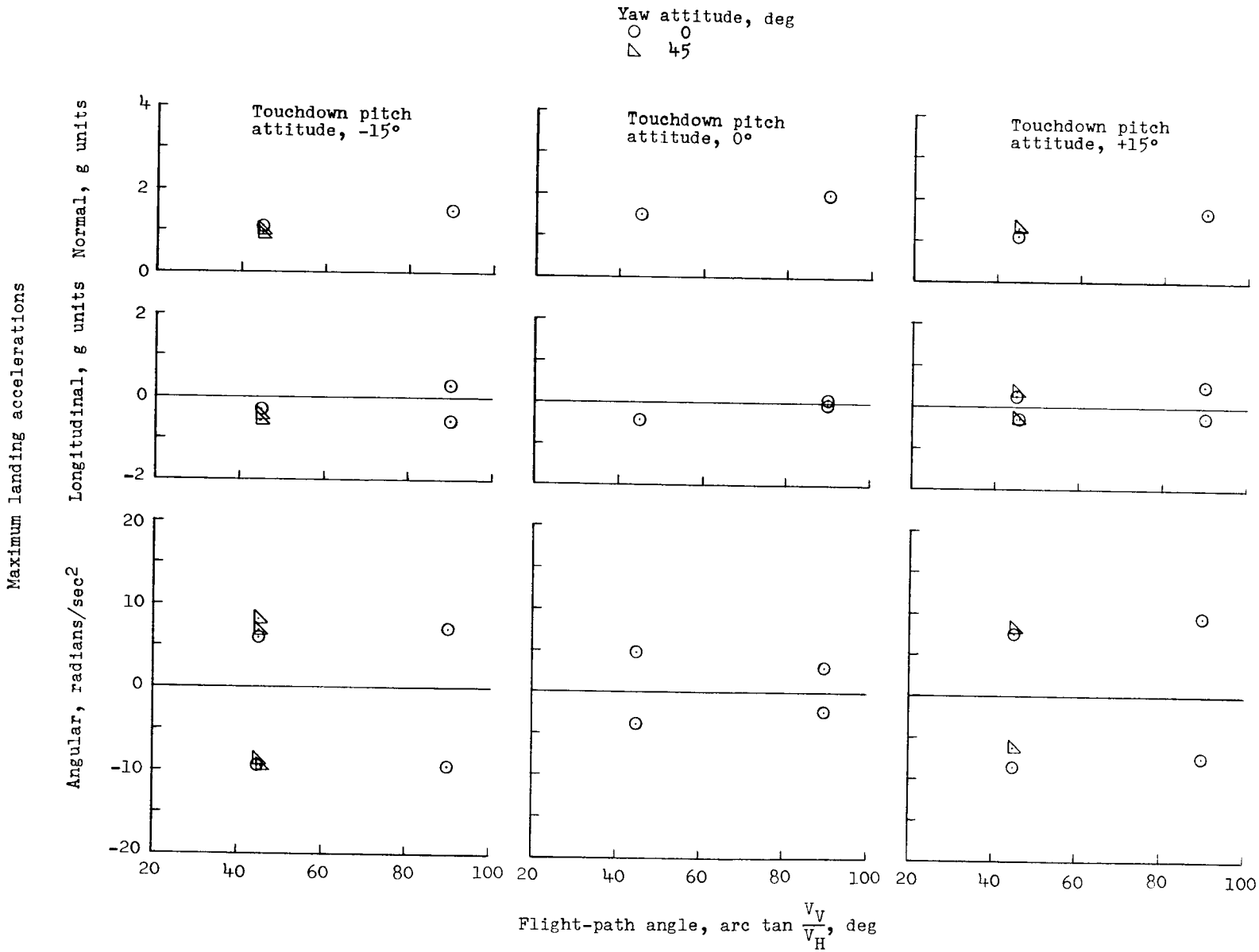

Figure 26.- Effect of flight-path angle on maximum accelerations and stability during landings at various attitudes on flat hard surface with symmetric five-point landing gear. Roll attitude, 0°.

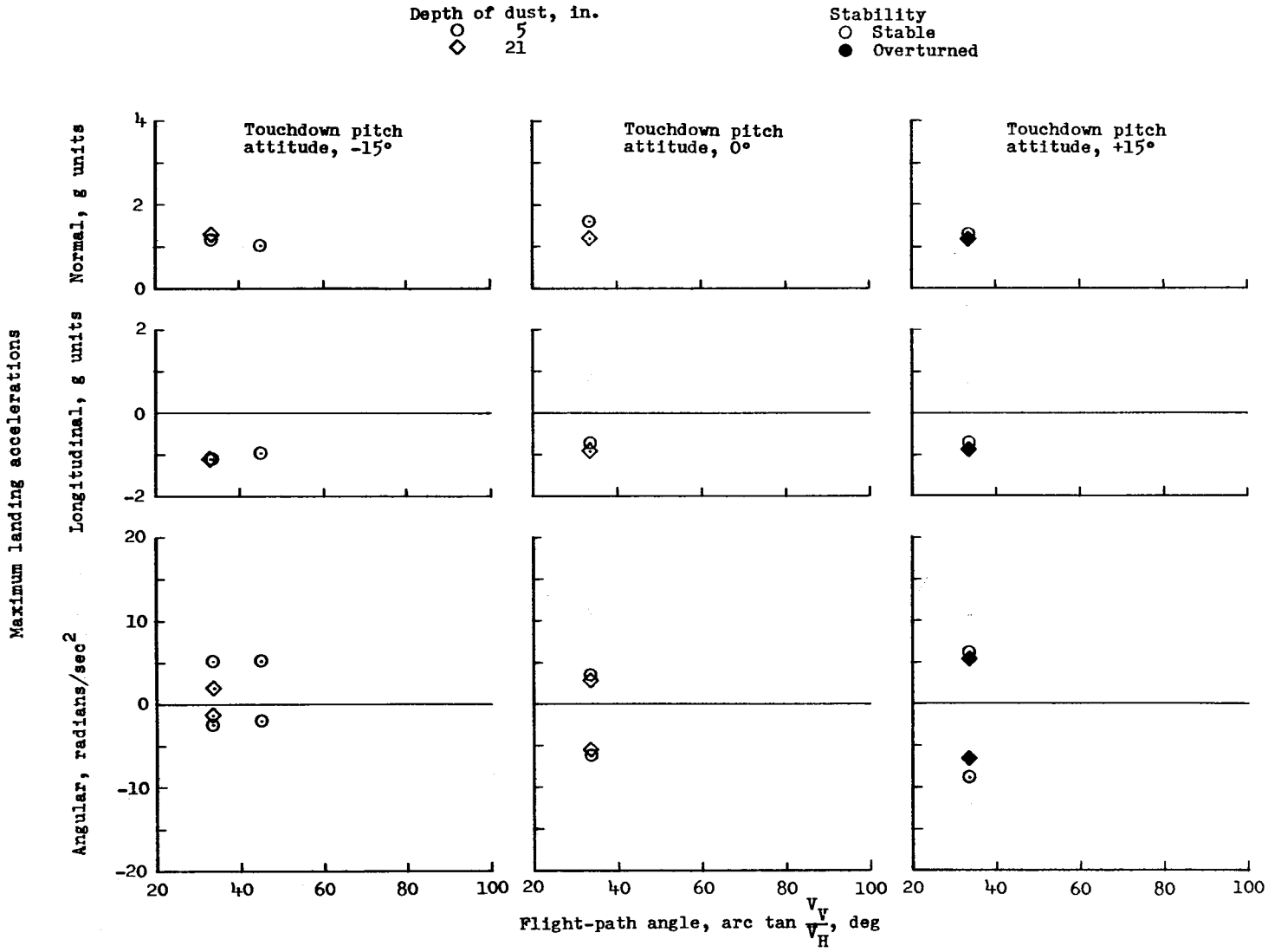

(a) Yaw attitude, 0°.

Figure 27.- Effect of symmetric five-point landing gear on maximum accelerations and stability for various landing conditions on flat dust overlay. Roll attitude, 0°.

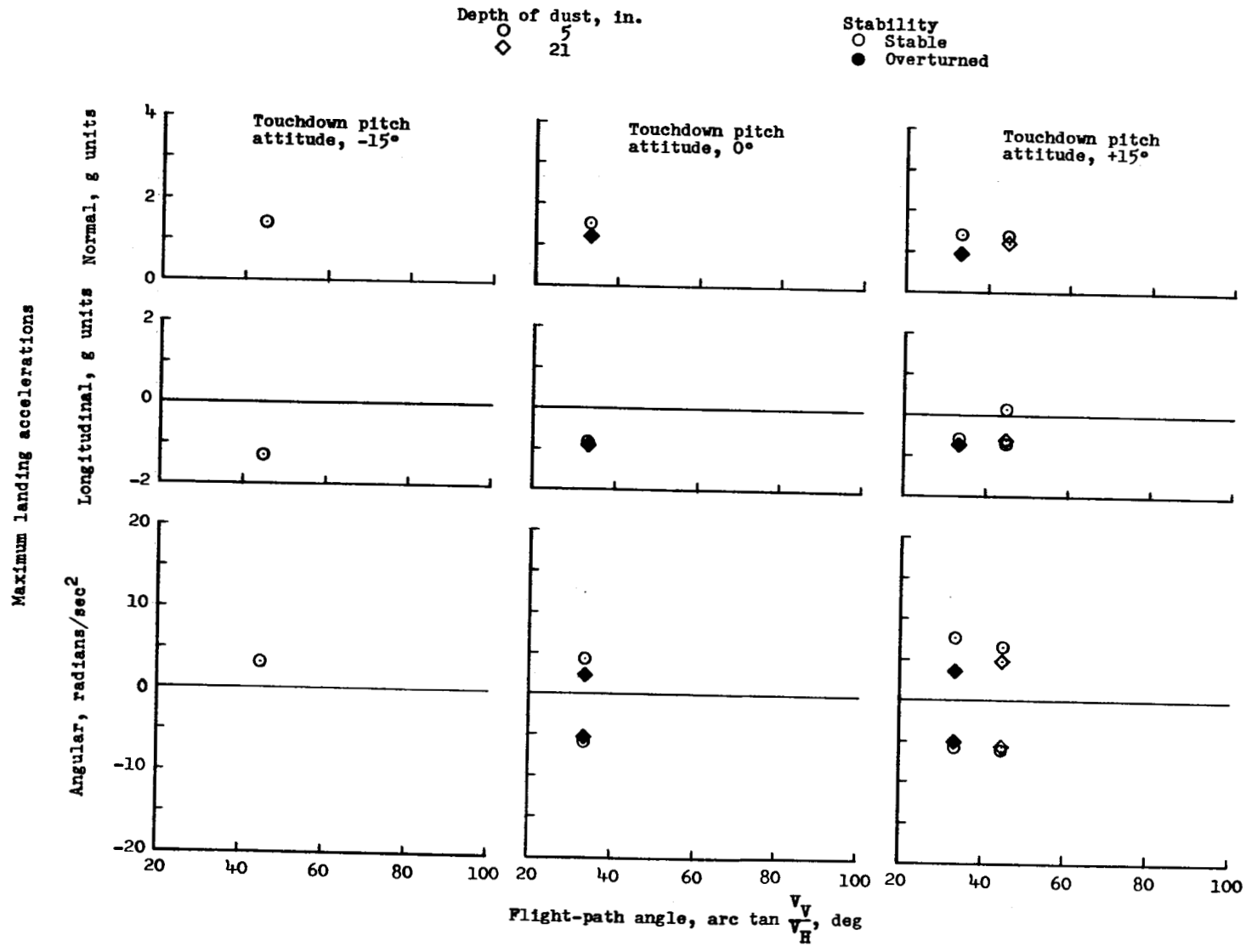

(b) Yaw attitude, 36°.

Figure 27.- Concluded.